P-57
2534

Polytechnic Institute of New York

WEBER RESEARCH INSTITUTE

POLY-MRI-1451-86
May 1986

FINAL TECHNICAL REPORT

ON

A MORPHOLOGICAL STUDY OF WAVES IN THE THERMOSPHERE USING DE-Z OBSERVATIONS

Submitted by

Stanley H. Gross
Spencer P. Kuo
Jerry Shmoys

(NASA-CR-176775) A MORPHOLOGICAL STUDY OF WAVES IN THE THERMOSPHERE USING DE-2 OBSERVATIONS Final Technical Report (Polytechnic Inst. of New York, Farmingdale.) 57 p HC A04/MF A01 CSCL 04A G3/46

N86-25070

Unclas 43355

Prepared for

National Aeronautics Space Administration

under

Grant NAG 5-479

ABSTRACT

Theoretical model and data analysis of DE-2 observations for determining the correlation between the neutral wave activity and plasma irregularities have been presented. The relationships between the observed structure of the sources, precipitation and Joule heating, and the fluctuations in neutral and plasma parameters are obtained by analyzing two measurements of neutral atmospheric wave activity and plasma irregularities by DE-2 during perigee passes at an altitude on the order of 300-350 km over the polar cap. Though it is still not clear whether one can conclude from these relationships that these perturbations arise from the Joule heating and precipitation, a theoretical model based on thermal nonlinearity (Joule heating) to give mode-mode coupling is developed to explore the role of neutral disturbance (winds and gravity waves) on the generation of plasma irregularities.

I. Introduction

NASA awarded a research grant (Grant No. NASA - NAG5-479) bearing the title "A Morphological Study of Waves in the Thermosphere Using DE-2 Observations", to the Polytechnic Institute of New York with Professor Stanley H. Gross as the Principal Investigator for one year beginning September 1, 1984. Under the support of this research grant, a number of investigations have been pursued. The investigation covered by the grant deals with data analysis of DE-2 observations for determining the correlation between the neutral wave activity and plasma irregularities. The aim of this study is to lead us to identify the source of perturbations, its structure and characteristics. Moreover, it is also our intention to develop theoretical models for understanding the coupling between the neutral waves and the plasma irregularities and for interpreting wave properties obtained from measurements, so as to characterize and interpret the observed disturbances.

At present, two measurements of neutral atmospheric wave activity and plasma irregularities by DE-2 during perigee passes at an altitude on the order of 300-350 Km over the polar cap are analyzed. They are for September 5, 1981 at 21:13 UT (day 81248) and October 15, 1981 at 0:51 UT (day 81288). Magnetic activity on the first day was modest. The kP was 2 in the seventh three hour period (18:00 to 21:00 UT) and 3_+ for the next three hour period (21:00 to 24:00 UT). The second case was at the start of a day that followed a day of considerable activity, October 14, 1981, in which kP reached 8. The kP index was 6_- from 21:00 to 24:00 UT on that day, but decreased to 3 from 0:00 to 3:00 UT on October 15, 1981, which interval covered the time of the second case. The effect of the previous day's activity was therefore quite evident in the measured data. The calculated Joule heating flux was found to be about twice as great on the October 15 pass than it was on the September pass.

Of interest here is the relationship between the observed structure of the sources, precipitation and Joule heating, and the fluctuations in the neutral and plasma parameters. Comparisons are made between perturbations of temperature, densities, electric field turbulence, neutral winds, neutral densities, between wavelike behavior in neutral densities and irregularities in ion density, all as related to these source structures and as related to each other. Though some relationships are found, it is not clear, as yet, whether these perturbations arise from the Joule heating and precipitation. They may also be associated with the structure of the convection cells at the time, and measurements are needed to clarify this point. A preliminary theoretical model based on thermal nonlinearity (Joule heating) is also developed to explore the role of neutral distrubance (winds and gravity waves) on the generation of plasma irregularities.

In section II of this report, the background of the research area is discussed. Section III presents the results of Data Analysis on the two measurements of DE-2 perigee passes. The theoretical study on the generation of plasma irregularities by collisional coupling of the neutral's velocity perturbations to the ionospheric plasma is given in Section IV.

II. Background of the Research Area

1.0 Background

Wave-like perturbations of constituents in the thermosphere are detected by measurements of the ionosphere by ground facilities and by instrumentation on board satellites measuring both neutral and ionospheric parameters. Perturbations of ionization are known as traveling ionospheric disturbances (TID's) (Hines, 1974; Georges, 1968; Yeh and Liu, 1974). A number of reports of large scale TID's (from hundreds to thousands of km) have suggested that they originate from high latitude regions during auroral substorms (Thome, 1968; Davis and de Rosa, 1969; Testud et al., 1975). These waves are believed to be caused by heat and momentum input into the atmosphere in the auroral zones from particle precipitation and Joule heating (Vickrey et al., 1982; Wickwar, et al., (1975). Their origins have been reviewed by Hunsucker (1982). Studies have also been made of these waves in association with magnetic storms by Richmond and Matsushita, (1975), Mayr and Volland, (1973) and Prolss, (1982).

Medium scale TID's (from tens to hundreds of km) are also observed, but their sources have not been well identified, though it is believed that meteorological phenomena may produce many of them. Larsen et al., (1982) have associated thunderstorms with these waves. Mastrantonio et al., (1976) have also associated these waves with jet streams in the atmosphere, and Bertin et al., (1978) have detected waves related to the jet stream. Auroral sources are also believed to be the cause of many of these disturbances (Georges, 1968).

The characteristics of all these are found to be generally in accordance with gravity wave theory (Hines, 1974) which has received some direct support from satellite measurements on board Explorer 32 (Dyson et al., 19700 and Atmospheric Explorer AE-C (Reber et al., 1975; Gross, 1980, 1984; Gross and

Huang, 1984; Gross et al., 1980, 1981a and b, 1982, and 1984; Huang et al., 1980; Hoegy et al., 1979). It is believed that the neutrals are perturbed by gravity waves as a result of localized sources of heating and momentum, and the neutrals, in turn, drive the ionization through collisions and temperature perturbations to produce these TID's. Gravity wave theory is concerned with two types of waves called gravity waves and acoustic-gravity waves. Acoustic-gravity waves make up the upper frequency branch and gravity waves the lower frequency branch of the hydrodynamical system in which both gravity (buoyancy) and compressibility act as restoring forces. The upper branch becomes identical to ordinary sound waves in the audio frequency range, but at its lowest frequencies, such waves are called "infrasonic waves." This branch has a lower cutoff frequency called the "acoustic cutoff frequency," and there is a cutoff region below this frequency which separates the two branches. The lower end of the cutoff band, which is the upper limit of the gravity wave branch, is called the "buoyancy frequency." The cutoff band is determined by the temperature and its vertical gradient and by the mean molecular mass of the medium, so that it varies somewhat with altitude. The cutoff band is relatively narrow, and periods within it range from about several minutes at low altitudes to from 10 to 15 minutes at higher altitudes, depending on temperature. The periods of gravity waves then range from the period of the buoyancy frequency to many hours, whereas those of acoustic-gravity waves range from the acoustic cutoff period to periods of seconds and less. In the gravity wave branch, long period waves usually have large horizontal wavelengths and shorter periods smaller wavelengths (Hunsucker, 1982; Morgan and Tedd, 1983).

Though fluctuations in ionization in the thermosphere have been measured both on the ground and by satellite borne instrumentation, the detection of

wave-like perturbations of neutral constituents in the thermosphere depends mostly on access by rockets and satellites. Radar is used only up to an altitude of about 100 km for neutrals. Satellite borne experiments have detected wave-like perturbations, both in total neutral density and temperature; for example, ESRO 4 (Prolss and Von Zahn, 1974a and b; Trinks and Mayr, 1976) OGO 6 (Reber and Hedin, 1974; Taeusch et al., 1971), AEROS-A (Chandra and Spencer, 1975 and 1976; Trinks et al., 1976), AE-C (Reber et al., 1975; Potter et al., 1976; and the various papers authored or co-authored by Gross in the references) and DE-2 (Hoegy et al., 1981). The density variation of individual species, namely, nitrogen, oxygen, helium and argon, have also been measured on board ESRO 4 , AEROS-A, AE-C, AE-E, and DE-2. Vertical velocity variations of these species have also been measured by AE-C, AE-E, and velocity variations by DE-2.

2.0 Source Problem and Energy Distribution

2.1 High Altitude Sources

Worldwide temperature increases in the thermosphere during magnetic disturbances have been observed by many researchers (Jacchia et al., 1967; Roemer, 1971; Reber and Hedin, 1974; Chandra and Spencer, 1976; and others). These disturbances are believed to be the source for many gravity waves observed in the thermosphere at mid and low-latitudes. The basis for this belief stems from observations of TID's by ionosounders (for example, Klostermeyer, 1969), by incoherent backscatter systems (Testud, 1970; Thome, 1968; Testud et al., 1975) and by Doppler sounders (Georges, 1968) that detect these distrubances moving toward the equator with speeds ranging from 200-700 m/sec. The relationships between thermospheric neutral particle effects and magnetic activity is inferred as well from the correlations of measured data

with storm events (Trinks et al., 1975 and 1976; Chandra and Spencer, 1975 and 1976). Waves have also been observed in association with auroral substorms in the evening section (Davis, 1971), though it has been suggested that some observed in the daytime may rise from the precipitation of soft particles about the cusp region (Trinks et al., 1975).

Two mechanisms in the auroral zone are considered to be the sources for the waves. These are Joule heating due to electrojet current dissipation in the ionosphere and momentum disturbances arising from the Lorentz force (Chimonas and Hines, 1970; Cole, 1971; Testud, 1970; Richmond and Matsushita, 1975; Roble et al., 1978; Richmond, 1979; Prölss, 1982) moving at supersonic speeds (Chimonas and Peltier, 1970) and heating due to particle precipitation (Hays et al., 1973). Nevertheless, it is generally accepted that the important mechanisms at work are mainly Joule heating and the Lorentz force in the E region (see Hunsucker, 1982). Gross et al., (1984), however, suggest that heating by particle precipitation in the F-region may also be at work producing waves observed by AE-C and AE-E. The structure of diffuse aurora caused by lower energy particles (Lui et al., 1982) reinforces this idea. Furthermore, Hunsucker, (1983) finds that there is no apparent correlation between TID's and magnetograms, except for large magnetic storms, suggesting that E region sources may not be at work when magnetic activity is below some threshold. New evidence of Morgan, (1983) may open such matters for further consideration. Anderson et al., (1982) propose that wind shears in the equatorial zone of the F region could also generate gravity waves in the thermosphere.

The energy input to the thermosphere from high latitudinal regions is believed to be significant relative to solar EUV input to the thermosphere (Ching and Chiu, 1973). The high latitude input is therefore of great importance to the physics of this layer, and the manner in which the energy is glo-

bally distributed to lower latitudes must be understood. Two major transport processes are favored; one is based on the thermospheric winds, the other on waves. It is very likely that both play a role (Klostermeyer, 1973; Chandra and Spencer, 1976; Mayr and Volland, 1972 and 1973). Waves distribute their energy through dissipation by viscosity, thermal conductivity, ion drag, wave-wave coupling and wind interactions. The extent of transport of energy and momentum by waves is of interest here. Richmond and Roble, (1979) estimate 2-4 x 10^{15} J can generate gravity waves capable of producing observed ionospheric disturbances at Millstone Hill and Arecibo incoherent scatter radar facilities.

2.2 Low Altitude Sources

Evidence that gravity waves in the thermosphere also originate in the lower atmosphere has been reported by Baker and Davies, (1969), Davies and Jones, (1971), Chimonas and Peltier, (1974) and Prasad et al., (1975). These investigators have found connection between the thermospheric disturbances and severe thunderstorm activity at mid-altitudes. Others have also found correlations with ground level microbarograms (Bowman and Shrestha, 1966; Khan, 1970; Herron and Montes, 1970; Shrestha, 1971a and b). These latter meteorologically-connected events appear to have shorter periods than the large scale events, from about 3 minutes to the order of 1 minute. Waves of such periods are so-called acoustic-gravity waves of the upper frequency branch of the mode. Coupling to the stratosphere has also been noted (Mason, 1968 and 1976; Fraser and Thorpe, 1976a and b). There have been observations of gravity waves in the thermosphere directly related to jet stream activity (Gertin et al., 1978), confirming a suggestion by Mastrantonio et al., (1976). Though evidence of correlation of jet stream activity and pressure fluctuations at the ground is plentiful, correlation with ionization variation would be an important

finding, because of implication as to the transport and distribution of energy and momentum.

It may be expected that meteorological sources are relatively common, though the effects of an individual event may be localized (Davies and Jones, 1971), in contrast with what is believed to be the global-like nature of disturbances generated in the auroral region. However, the common presence of waves of scale sizes ranging from about 80 km to several hundred kilometers observed in satellite data (Gross et al., 1980 and 1981b, 1982; Gross and Huang, 1984) suggest that considerable meteorologically generated disturbances reach the thermosphere. In this regard, it is important to know what part of the disturbances are associated with auroral activity. Meterological events (not all of which appear to produce waves in the thermosphere) may cause the transport of energy into the thermosphere in amounts not inappreciable relative to the solar EUV (Hines, 1965; Testud, 1970; Lindzen and Blake, 1970) If this much energy can reach the thermosphere, after possible partial reflection at some level and/or possible evanescence in some altitude region, such phenomena may also be indicative of the deposition of much more energy below the thermosphere. The chemistry and dynamics of the lower thermosphere, mesophere, and stratosphere can be significantly modified in such events. The interplay of tropospheric phenomena and these upper regions is of importance. One aspect may bear on the generation of turbulence and mixing up to the turbopause. Wave effects on the turbopause may also be important because of the effect of the altitude of the turbopause on the specie distribution above it (Chandra and Herman, 1969; Chandra and Spencer, 1976).

III Measured Data and Analyses

The orbital paths over the polar region are shown in Figure 1 for the two passes. These are plots of invariant latitude against magnetic local time. The path for the second day for orbit 1071 on day 81288 passes closer to the magnetic pole than that of the first day 81248, orbit 492.

Figure 2 is a plot vs time in hours and minutes UT, as well as other ephemeris information, of the variation of various parameters measured by the LAPI, VEFI, LANG and WATS instruments for orbit number 492 on day 81248. The top panel contains particle precipitation information in the form of the energy flux for electrons with energies as given by the logarithmic scale on the left. The flux is not readily obtained from the graph, since the original data utilized a color scale: however, the darker the appearance, the higher the flux. The highest possible flux of the scale is 1 erg/cm^2-sec-sr-ev. The second panel is the turbulence in the electric field plotted on a logarithmic scale for the frequency band 8-16 HZ, shown as dots, and the 4-16 kHz band, shown as 0's. The rise in the turbulence is quite evident at about 21:13 UT, at which time spikes in the precipitation flux of 3-4 kev electrons are quite evident in the LAPI data. These spikes are probably upward currents, and the region is believed to be the cusp. The third panel is a plot of electron temperature. The discontinuity and perturbation at 21:13 UT confirms the cusp location. The ion density is shown in the fourth panel, and a drop in density as well as irregularities are observed to occur at about the same time. The fifth and bottom panel contains both the horizontal and vertical neutral winds, coded H and V, respectively. Note the rise in the horizontal wind at about 21:13 UT. Also note the wavelike variations in both wind components. The horizontal wind here is across the orbital pass and is mostly east-west. The step in the horizontal wind is not a true discontinuity. It is the result of the change in direction, as

designated, on passing over the geographic pole (note the geographic latitude 89.98^0).

Figure 3 is the same as Figure 2, but for orbit 1071 on day 81288. The extended region of precipitaiton is quite evident and contrasts with that in Figure 2. Note the spikey nature of the precipitation at about about 00;50 UT which is also associated with the rise in the electric field turbulence, the change in electron temperature and ion density there, as well as the rise in the horizontal wind. It is believed that this is the cusp region. There is also considerable turbulence before this time which undoubtedly relates to the borad extent of the precipitation. The winds, electron temperature and ion density also exhibit considerable variation throughout, and the winds appear quite wavelike in their variation.

Figure 4 contains plots of the variations in the magnetic field components and one electric field component, the x component which is along the spacecraft velocity vector, vs time in hours and minutes UT for the two days, 81248 on the left and 81288 on the right. Also on each of the graphs is a plot of the integrated downward Joule heating flux, designated SY in the figure. Note that the center of the flux is at 21:13 UT on day 81248 which is the time when the orbital path cuts through the cusp, and at 0:50 UT on day 81288, also the time of travel through that region. The peak Joule heating flux is about 50 mW/m^2 on day 81248, whereas it is about double, 100 mW/m^2 on 81288. The duration of the Joule heating pulse in orbit at the 10% level, $5mW/m^2$, is about 53 seconds, about 400 km in distance along the orbital track for day 81248. The Joule heating pulse for day 81288 is actually like a double pulse. Its overall duration at the 10% level, 12 mW/m^2 is about 120 seconds, or a distance of about 900 km along the orbital track.

Figure 5 is a plot of the densities of oxygen, nitrogen, ions and electron

temperature vs time in seconds UT and other parameters. Samples are roughly 1 second apart. The upper graph is fo day 81248, whereas the lower is for day 81288. These plots show the electron temperature and ion density variations in greater detail than those in Figures 2 and 3. For 81288 on the bottom, note the dip in the oxygen density, the rise in the nitrogen density, the increase in electron temperatures and decrease in ion density, all at about the same time, the time interval during Joule heating, about 0:50 UT. Note also the more gradual fluctuation of the neutral gas densities as contrasted with the irregularity of the ion density and electron temperature. the neutral density changes are not very evident for the Joule heating region 21:13 UT for 81248, though there is some small decrease in oxygen and increase in nitrogen densities. The more gradual fluctuation of the neutral densities in contrast with irregularities in the ion density and electron temperature is also quite apparent.

Figure 6 is a plot vs time in seconds UT of the fluctuations in the densities of the ions, oxygen and nitrogen for day 81248. The fluctuations are obtained from the densities shown in Figure 5 by passing the logarithm of the densities through a digital bandpass filter with a lower cutoff frequency of 0.005 Hz, which corresponds to about 1500 km scale size along the orbital track, and an upper cutoff frequency of 0.833 Hz, which corresponds to about 90 km. Thus, the filter passes components of scale size between these limits. The upper cutoff is used to filter out noise in the data. Some of the features overlap. Thus, the negative excursion of the oxygen and electron density fluctuations and the rise in the nitrogen density fluctuation at a point past the 76350 second tick marker is associated with the peak in the Joule heating. Other both smaller and larger scale features match, though there are still some differences. Regions seem to correlate or anti-correlate in part. The fluctuations are the relative fluctuations with respect to the background. Relative ion density

fluctuations as large as 43% are obtained, though the mean level is closer to 20% The oxygen-relative fluctuations are on the order of 3%, whereas that of nitrogen is closer to 3.5%

Figure 7 shows the FFT power spectra of the fluctuations in Figure 6 plotted against wave period rather than frequency. The only spectral feature that appears common in the three spectra for this day, 81248, is one with a period of about 100 seconds which corresponds to a spatial structure of about 750 km. This size is roughly twice the scale size of the 10% level of the Joule heating pulse in Figure 4 for day 81248. This relationship could still be accidental.

Figure 8 is the same as Figure 6, but for day 81288. The same filter has been used. The feature associated with Joule heating may be seen just beyond the 2977 seconds tick mark. Other features appear to correlate to some extent, though there is still considerable differences.

Figure 9 shows the power spectra plotted vs period for the fluctuations of Figure 8, which is for day 81288. Spectral features appear to correlate somewhat at about 110 to about 128 seconds, 825 to 900 km on the orbital track. This scale size corresponds to the width at the 10% level of the Joule heating pulse. /In the following, we present an/ The connection may again be accidental. The large peaks in the oxygen and nitrogen spectra at about a period of 500 seconds is spurious and due to the finite size of the data samples.

IV Theoretical Analysis and Modeling Studies

Modeling studies are necessary to guide the interpretation of measured data. Since the coupling of neutrals and ionization is of interest, it is necessary to take into account more than one fluid. Such studies have been made for the sourceless linear case (for example, Dudis and Reber, 1976; Gross and Eun, 1976 and 1978; Del Genio et al., 1979). Since sources and their characteristics are of interest as well, source driven models must be treated. Such studies, however, were only made for atmospheres of just one species (for example, Chimonas and Hines, 1970; Richmond and Matsushita, 1975). At the Polytechnic we have been studying the problem of multiple constituents or fluids with sources, particularly for two species (Eun and Gross, 1976a and b; Gross and Eun, 1976, 1978). No extensive analytical treatment has as yet been made for more than two species, though with the assumption of truly minor species, one may treat the atmosphere as a two-fluid problem with one fluid for the major species and the other any of the minor species. Mayr and Volland, (1976) and Mayr et al., (1982 and 1983) have modeled the problem on a computer for propagation in a spherical geometry for a number of neutral constituents with losses. No full treatment of ionospheric plasma in a magnetic field coupled to neutral species with sources has as yet been made.

In the following, we present an analysis to show that plasma irregularities can be generated by collisional coupling of the velocity perturbations of the neutral waves in the neutrals to the ionosphere plasma. The thermal nonlinearity gives the mechanism for mode-mode coupling and provides a channel for transfer of the space-time oscillating perturbations into disturbances having only spatial oscillations (irregularities). In order to simplify the analysis, geometry corresponding to equatorial latitude is chosen. The application of the analysis is then focused on explaining the spread F (ESF) phenomenon.

1.0 Coupling of Netural and Ionospheric Distrubances

The rising and the subsequent descending of the ionosphere after sunset have been noted as the striking symptom of the onset of ESF (see, e.g., Herman, 1966; Rastogi and Woodman, 1978). These upward and downward motions of the ionosphere are controlled by the E region dynamo. During the reversal of neutral winds, a wind shear may form and become the source of neutral waves (Hines, 1967, 1971). The formation of a wind shear in the F region was invoked by Anderson et al. (1982) as the hypothesized source of in-situ neutral waves for the local seeding of ESF. No wind shear in the F region was seen in the ALTAIR data, however, at time of wave structure formations. The wind shear required for the generation of in-situ neutral waves in the F region was estimated to be, at least, 16 m/sec/Km based on the criterion that $R_i \lesssim 0.25$, where R_i is the Richardson number. While this required wind shear seems to be large in the F region, much greater wind shear can exist in the E region.

Intense neutral waves produced, for instance, by the solar terminator (Beer, 1973b) or a wind shear in the E region are suggested in the present paper as the potential local coherent sources of exciting large-scale ($\gtrsim$ tens of kilometers) ionospheric density irregularities and forced ion acoustic modes. Ionospheric density irregularities are driven by the thermal pressure force that stems from the collisional dissipation of both the neutral wave and the excited ion acoustic modes via plasma-neutral collisions. This process, as shown below, relies on large plasma-neutral collisions. It thus represents an efficient coupling between the neutral and the ionospheric disturbances in the E region rather than in the F region. However, the electric field perturbations associated with the large-scale field-aligned E region irregularities can map along the geomagnetic field lines up to the F region (Farley, 1960) and, consequently,

provide the initial plasma density perturbations for the subsequent excitation of Rayleigh-Taylor instability.

1.1 Neutral wave as a pump

Neutral waves, whose intensity is evaluated in terms of the neutral velocity perturbation ($\underset{\sim}{V}_n$) in the following analysis, can transfer their momentum and energy to the charged particles through collisions. A plasma instability can be excited at the expense of the neutral wave. Whether the induced ionospheric disturbances can significantly affect the F region dynamics depends upon the characteristics of the instability such as the thresholds and the growth rates. The proposed neutral-ionosphere coupling process is analyzed by fluid equations, because the scale lengths of plasma modes are greater than the ion gyroradii by several orders of magnitude. The nighttime E region is approximated as a homogeneous plasma imposed by a uniform magnetic field.

The two plasma modes under consideration are field-aligned low frequency mode and a forced ion acoustic mode that are parametrically excited by the neutral wave. This three-wave interaction process can be conveniently described by the following wave frequency (ω) and wave vector ($\underset{\sim}{k}$) marching relations:

$$R_e(\omega_o) = R_e(\omega_s) + R_e(\omega_a)$$

$$\underset{\sim}{k}_o = \underset{\sim}{k}_s + \underset{\sim}{k}_a$$

where $R_e(\omega)$ means the real part of ω the subscripts o, s, and a denote the neutral wave, the low frequency mode, and the ion acoustic mode, respectively. It will be shown that $R_e(\omega_s) \ll R_e(\omega_a)$ and the low frequency mode is nearly a zero frequency (or purely growing) mode. The forced ion acoustic mode is so termed because its frequency is determined by that of the neutral wave. There-

fore, this frequency may far deviate from the characteristic frequency (~a few kHz) of the ion acoustic waves in the ionosphere.

The perturbations in plasma density (n), velocity ($\underset{\sim}{V}$), and electric field ($\underset{\sim}{E}$) caused by the low frequency mode (or ion acoustic mode) are represented by $N_s(\delta N_a)$, $\underset{\sim}{V}_s(\delta \underset{\sim}{V}_a)$, and $\underset{\sim}{E}_s(\delta \underset{\sim}{E}_a)$, respectively. The plasma-neutral collision frequency has the expression of $\nu_{pn} = \nu_{pno}(1 + \delta N_n/N_{no})$ with the neutral density perturbation (δN_n) taken into account, where p = e (electrons) or i (ions), N_{no} is the unperturbed neutral density, and ν_{pno} is the collision frequency in the absence of δN_n.

1.2 Large-scale Field-aligned Ionospheric Irregularities

The coupled mode equation for the low frequency mode (i.e., the large-scale field-aligned ionospheric irregularities) can be derived from the following linearized electron and ion equations.

They are:

(I) Momentum equations

$$M_e N_o \frac{\partial}{\partial t}\underset{\sim}{V}_{se} = -\nabla(T_{eo}N_s + N_o\delta T_e) + N_o e(\underset{\sim}{E}_s + \frac{1}{C}\underset{\sim}{V}_{se} \times \hat{z} B_o) - M_e N_o \nu_{eno}\underset{\sim}{V}_{se} - M_e N_o \frac{\delta N_n}{N_{no}}\delta \underset{\sim}{V}^*_{ae}\nu_{eno} + M_e \delta N_a^* \underset{\sim}{V}_n \nu_{eno} \tag{1}$$

$$M_i N_o \frac{\partial}{\partial t}\underset{\sim}{V}_{si} = -\nabla(T_{io}N_s + N_o\delta T_i) + N_o e(\underset{\sim}{E}_s + \frac{1}{C}\underset{\sim}{V}_{si} \times \hat{z} B_o) - M_i N_o \nu_{ino}\underset{\sim}{V}_{si} - M_i N_o \frac{\delta N_n}{N_{no}}\delta \underset{\sim}{V}^*_{ai}\nu_{ino} + M_i \delta N_a^* \underset{\sim}{V}_n \nu_{ino} \tag{2}$$

where $M_e(M_i)$, e, $T_{eo}(T_{io})$, N_o, and $\underset{\sim}{B}_o$ ($= \hat{z}B_o$) are the electron (ion) mass, the electric charge, the unperturbed electron (ion) temperature, the unperturbed plasma density, and the earth's magnetic field taken to be the z axis of a

rectangular coordinate system; the last two terms on the RHS of (1) and (2) come from the coupling of the gravity wave (δN_n and $\underset{\sim}{V}_n$) and the ion acoustic mode ($\delta \underset{\sim}{V}_a$); the electron and the ion temperature perturbations (δT_e and δT_i) result from the thermal effect described by the heat source term in the energy equation;

(II) Energy equations

$$\frac{3}{2}N_o \frac{\partial}{\partial t}\delta T_e + N_o T_{eo} \nabla \cdot \underset{\sim}{V}_{se}$$

$$= \nabla\cdot(R_{\parallel}^{e}\nabla_{\parallel}+R_{\perp}^{e}\nabla_{\perp})\delta T_e - 3N_o\nu_{eno}\frac{M_e}{M_n}(\delta T_e - \delta T_n) - n_o\nu_{eno}M_e(\delta \underset{\sim}{V}_{ae}^{*}\cdot \underset{\sim}{V}_n) \tag{3}$$

$$\frac{3}{2}N_o \frac{\partial}{\partial t}\delta T_i + N_o T_{io} \nabla \cdot \underset{\sim}{V}_{si}$$

$$=\nabla\cdot(R_{\parallel}^{i}\nabla_{\parallel}+R_{\perp}^{i}\nabla_{\perp})\delta T_i - 3N_o\nu_{ino}\frac{M_i}{(M_i+M_n)}(\delta T_i - \delta T_n) - N_o\nu_{ino}M_i(\delta \underset{\sim}{V}_{ai}^{*}\cdot \underset{\sim}{V}_n) \tag{4}$$

where M_n and δT_n are the neutral mass and the neutral temperature perturbation, respectively; the first term on the RHS of (3) and (4) represents the parallel and the cross-field heat conduction rates, the second term is the cooling rate due to plasma- neutral collisions, and the last one is the heat source term contributed form the collisional dissipation of both the gravity wave and the ion acoustic mode;

(III) Continuity equations

$$\frac{\partial}{\partial t}N_s + \nabla \cdot N_o \underset{\sim}{V}_{se} = 0 = \frac{\partial}{\partial t}N_s + \nabla \cdot N_o \underset{\sim}{V}_{si} \tag{5}$$

where the quasi-neutrality condition, viz., $N_{se} \simeq N_{si} = N_s$, has been used; further, it is reasonable to assume that

(IV)

$$\delta T_i \simeq \delta T_n \tag{6}$$

if the ion mass is not very different from the neutral mass. Therefore, the cooling term in the ion energy equation disappears with this assumption.

We also assume that the perturbations associated with the low frequency mode have a space-time dependence of the $\exp[i(k_s x - \omega_s t)]$ form, where $\omega_s = \omega_r + i\gamma$ and $\omega_r(\gamma)$ is the real frequency (growth rate) of the low frequency mode. This mode has a field-aligned nature, viz., its wave vector is orthogonal to the earth's magnetic field ($\underset{\sim}{B}_o = \hat{z}B_o$) and is chosen to be the x axis of the coordinate system. Replacing $\nabla(= \hat{x}\partial/\partial x)$ and $\partial/\partial t$ in (1)-(6) by $i\underset{\sim}{k}_s (= i\hat{x}k_s)$ and $-i\omega_s$ and eliminating $\delta T_e, \delta T_i$, $\underset{\sim}{V}_{se}, \underset{\sim}{V}_{si}$, and $\underset{\sim}{E}_s$ from these equations, we obtain the following coupled mode equation for the field-aligned ionospheric irregularities

$$\left\{(\gamma - i\omega_r)[\gamma - i\omega_r + \nu_{ino} + \frac{M_e}{M_i}\nu_{eno}] + \Omega_i\left(\frac{\Omega_e}{\gamma + \nu_{eno}} + \frac{\Omega_i}{\gamma + \nu_{ino}}\right)\right.$$
$$\left. + \frac{2}{3}\frac{k_s^2}{M_i}\left(\frac{T_{eo}}{\bar{\gamma}_e} + \frac{T_{io}}{\bar{\gamma}_i} + 2\frac{M_e}{M_n}\frac{\nu_{eno}}{\bar{\gamma}_e}\frac{T_{eo}}{\bar{\gamma}_i}\right) + k_s^2 C_s^2\right\}\left(\frac{N_s}{N_o}\right)$$
$$= \frac{2}{3}k_s^2\left[\nu_{eno}\left(\frac{M_e}{M_i}\right)\frac{\delta\underset{\sim}{V}^*_{ae}}{\gamma_e} + \left(2\frac{M_e}{M_n}\frac{\nu_{eno}}{\bar{\gamma}_e} + 1\right)\frac{\nu_{ino}}{\bar{\gamma}_i}\,\delta\underset{\sim}{V}^*_{ai}\right] \cdot \underset{\sim}{V}_n$$

$$- ik_s\frac{\delta N_n}{N_n}\left[\nu_{eno}\left(\frac{\Omega_i}{\gamma + \nu_{eno}}\delta V_{aey} - \frac{M_e}{M_i}\delta V^*_{aex}\right) - \nu_{ino}\left(\frac{\Omega_i}{\gamma + \nu_{ino}}\,\delta V^*_{aiy} + \delta V^*_{aix}\right)\right]$$

$$- ik_s\left[\nu_{eno}\left(\frac{M_e}{M_i}V_{nx} - \frac{\Omega_i}{\gamma + \nu_{eno}}V_{ny}\right) + n_{ino}\left(V_{nx} + \frac{\Omega_i}{\gamma + \nu_{ino}}V_{ny}\right)\right]\left(\frac{\delta N^*_a}{N_o}\right) \tag{7}$$

where $\Omega_e(\Omega_i)$ is the electron (ion) gyrofrequency;

$\bar{\nu}_e = \nu + 2(M_e/M_n)\nu_{eno} + k_s^2 V_{te}^2/(\Omega_e^2 + \nu_e^2)]\nu_e$ and $\bar{\gamma}_i = \gamma + [k_s^2 V_{ti}^2/(\Omega_i^2 + \nu_i^2)]\nu_i$,

where $V_{te}(V_{ti})$ and $\nu_e(\nu_i)$ are the electron (ion) thermal velocity and the effective electron (ion) collision frequency, respectively. The three terms,

$$2(M_e/M_n)\nu_{eno}\,,\ \nu_e k_s^2 V_{te}^2/(\Omega_e^2 + \nu_e^2),\ \text{and}\ \nu_i k_s^2 \nu_{ti}^2/(\Omega_i^2 + \nu_i^2)$$

are the electron cooling rate due to electron-neutral collisions, the electron cross-fleld heat conduction loss rate, and the ion cross-fleld heat conduction loss rate, respectively. The RHS of (7) represents the nonlinearity of causing ionospheric irregularities, viz., the collisional dissipation of the gravity pump wave and the forced ion acoustic mode.

1.3 Forced Ion Acoustic Mode

The forced ion acoustic mode is the "high frequency" sideband excited parametrically by the gravity pump wave. Since its frequency is determined by the beat frequency of the gravity wave and the low frequency mode, it is not necessarily the characteristic frequency of the acoustic waves. The electron and ion equations that are required for the derivation of the coupled mode equation for the forced ion acoustic mode include the continuity equations and the momentum equations.

For simplicity, the forced ion acoustic mode is assumed to propagate along the earth's magnetic field; viz., $\underset{\sim}{k}_a = \hat{z}k_a$. This assumption is quite reasonable in the E region where $\nu_{in_o} >> \Omega_i$ indicating that the ion dynamics can be treated approximately as in the unmagnetized case. With the $\exp[i(k_a z - \omega t)]$ type of perturbations, the linearized electron and ion equations can be written as:

(I) Continuity equations

$$-\omega_a \delta N_a + iN_o k_a \delta V_{aez} = 0 = -i\omega_a \delta N_a + iN_o k_a \delta V_{aiz} \qquad (8)$$

namely,

$$\delta V_{aez} = \delta V_{aiz} = \delta V_{az} ,$$

(II) Momentum equations

$$M_e N_o (-i\omega + \nu_{eno}) \, \delta \underset{\sim}{V}_{ae}$$

$$= i\hat{Z} k_a T_{eo} \delta N_a - N_o e(\hat{Z}\delta E_a + \frac{1}{c} \delta \underset{\sim}{V}_{ae} \times \hat{Z} B_o) -$$

$$M_e N_o \nu_{eno} \frac{\delta N_n}{N_{no}} \underset{\sim}{V}^*_{se} + M_e N^*_s \nu_{eno} \underset{\sim}{V}_n \qquad (9)$$

$$M_i N_o (-i\omega + \nu_{ino}) \, \delta \underset{\sim}{V}_{ai}$$

$$= - i\hat{Z}_a T_{io} \, \delta N_a + N_o e(\hat{Z}\delta E_a + \frac{1}{c} \delta \underset{\sim}{V}_{ai} \times \hat{Z} B_o) -$$

$$M_i N_o \nu_{ino} \frac{\delta N_n}{N_{no}} \underset{\sim}{V}^*_{si} + M_i N^*_s \, \nu_{ino} \underset{\sim}{V}_n \qquad (10)$$

where $\omega = \omega_a + i\gamma$. The quasi-neutrality approximation, $\delta N_i \sim \delta N_e = \delta N_a$, has been used in (8) - (10).

Eliminating V_{sez} , V_{siz} , and δE_a from the z components of (1), (2), (9) and (10) leads to

$$\left\{ - \frac{i}{\omega_a} (\omega_a^2 - k_a^2 C_s^2) + (\nu_{ino} + \frac{M_e}{M_i} \nu_{eno}) - \left[\frac{\nu_{ino}^2}{\gamma + \nu_{ino}} + \frac{M_e \nu_{eno}^2}{M_i (\gamma + \nu_{eno})} \right] \right.$$

$$\left. \left(\frac{\delta N_n}{N_{no}} \right)^2 \right\} \delta V_{az} = (\nu_{ino} + \frac{M_e}{M_i} \nu_{eno}) \frac{N^*_s}{N_o} V_{nz} - \left[\frac{\nu_{ino}^2}{\gamma + \nu_{ino}} + \frac{M_e \nu_{ino}^2}{M_i (\gamma + \nu_{eno})} \right] \frac{\delta N_a}{N_o} V^*_{nz} \frac{\delta N_n}{N_{no}} \qquad (11)$$

with the aid of (8), where C_s is the ion acoustic velocity. Under the assumption that $R_e(\omega_a) \geq \gamma$ and $\gamma << \nu_{ino} < \nu_{eno}$ and since

$$\omega_a^2 \simeq k_a^2 C_s^2$$

then (11) reduces to

$$\delta V_{az} \sim \frac{N_s^*}{N_o} V_{nz} \left[1 - \left(\frac{\delta N_n^*}{N_o} - \frac{k_a V_{nz}^*}{\omega_a}\right)\right]^{-1} \simeq \frac{N_s^*}{N_o} V_{nz} \tag{12}$$

Solving (9) and (10) for δV_{aex}, δV_{aex}, δV_{aey} and δV_{aiy}, respectively, we get the following results:

$$\delta V_{aex} \simeq \left(\frac{\nu_{eno}}{\Omega_e}\right)^2 \left(\frac{N_s^*}{N_o} V_{nx}\right) - \left(\frac{\nu_{eno}}{\Omega_e}\right)\left(\frac{N_s^*}{N_o} V_{ny}\right) \tag{13}$$

$$\delta V_{aey} \simeq \left(\frac{\nu_{eno}}{\Omega_e}\right)^2 \left(\frac{N_s^*}{N_o} V_{ny}\right) + \left(\frac{\nu_{eno}}{\Omega_e}\right)\left(\frac{N_s^*}{N_o} V_{nx}\right) \tag{14}$$

$$\delta V_{aix} \simeq \alpha \frac{N_s^*}{N_o} V_{nx} + \beta \frac{N_s^*}{N_o} \left(\frac{\nu_{eno}}{\Omega_e}\right) V_{ny} \tag{15}$$

and

$$\delta V_{aiy} \simeq \alpha \frac{N_s^*}{N_o} V_{ny} - \beta \frac{N_s^*}{N_o} V_{nx} \tag{16}$$

where $\alpha = 1$ and $\beta = \Omega_i/\nu_{ino}$ for $\Omega_i \ll \nu_{ino}$ in the E region; $\alpha = (\nu_{ino}/\Omega_i)^2$ and $\beta = \nu_{ino}/\Omega_i$ for $\Omega_i \gg \nu_{ino}$ in the F region. Since $(\nu_{eno}/\Omega_e) \sim 10^{-2}\ (10^{-6})$ and $(\Omega_i/\nu_{ino}) \sim 10^{-1}\ (10^{+2})$ in the E(F) region, Equations (12)-(16) yield a simple coupled mode equation for the forced ion acoustic mode, viz.,

$$\delta \underset{\sim}{V}_{ai} \simeq \left(\frac{N_s^*}{N_o}\right) \underset{\sim}{V}_n \gg \delta \underset{\sim}{V}_{ae} \tag{17a}$$

for $\Omega_i \ll \nu_{ino}$ in the E region, or,

$$\delta \underset{\sim}{V}_{ai} \simeq \delta(\underset{\sim}{V}_{n\perp} \times \hat{z}) \left(\nu_{ino}/\Omega_i\right) \left(\frac{N_s^*}{N_o}\right) + \hat{Z} \left(\frac{N_s^*}{N_o}\right) V_{nz} \gg \delta \underset{\sim}{V}_{ae} \tag{17b}$$

for $\Omega_i \gg \nu_{ino}$ in the F region. It has seen that if the neutral wind blows dominantly along the earth's magnetic field (i.e., $\underset{\sim}{V}_n \simeq \hat{Z} V_{nz}$), $\delta \underset{\sim}{V}_{ai}$ in the F region is

approximately equal to $\delta \underset{\sim}{V}_{ai}$ in the E region. Otherwise, the latter is greater than the former by a large factor of Ω_i/ν_{ino} (F region parameters).

2.0 Excitation of the instability

Under the assumptions that $\nu_{eno} > \nu_{ino} >> \gamma$ and $k_a^2 C_s^2 >> \omega_r^2$, can be separated into the following two equations

$$\omega_r \simeq \frac{V_{nx}}{(|\omega_a|/k_s)} \frac{V_n}{(|\omega_a|/k_a)} R_e(\omega_a) << R_e(\omega_a) \tag{18}$$

and

$$\left\{\gamma\left[\nu_{ino} + \frac{\Omega_e \Omega_i}{\nu_{eno}} + \frac{2}{3}\frac{k_s^2}{M_i}\left(\frac{T_{eo}}{\overline{\gamma}_e} + \frac{T_{io}}{\overline{\gamma}_i} + 2\frac{M_e}{M_n}\frac{\nu_{eno}}{\overline{\gamma}_e}\frac{T_{eo}}{\overline{\gamma}_i}\right)\right] + k_s^2 C_s^2\right\}\frac{n_s}{n_o}$$

$$= \frac{2}{3}k_s^2\left[\nu_{eno}\frac{M_e}{M_i}\frac{\underset{\sim}{V}^*_{ae}}{\overline{\gamma}_e} + \left(2\frac{M_e}{M_n}\frac{\nu_{eno}}{\overline{\gamma}_e} + 1\right)\frac{\nu_{ino}}{\overline{\gamma}_i}\delta\underset{\sim}{V}^*_{ai}\right]\cdot\underset{\sim}{V}_n \tag{19}$$

According to (18) and assuming that $R_e(\omega_a) > \gamma$, $\omega_r (= R_e(\omega_s))$ is less than $R_e(\omega_a)$ by at least four orders of magnitude since

$$|\omega_a|/k_s \sim |\omega_a|/k_a \sim C_s \sim 10^3 \text{ m/sec.}$$

Therefore, this result shows that the low frequency field-aligned mode can be considered to be a zero-frequency mode and that the frequency ($R_e(\omega_a)$) of the forced ion acoustic mode is determined by that (ω_o) of the neutral wave, i.e., $R_e(\omega_a) = \omega_o$.

Based on (17a,b) and the assumption that $\nu_{ino}/\overline{\gamma}_i$ and $\nu_{eno}/\overline{\gamma}_e >> 1$, it becomes clear in (19) that the neutral-electron interaction ($\approx \nu_{eno}\delta\underset{\sim}{V}^*_{ae}\cdot\underset{\sim}{V}_n$) has a negligibly small effect on the excitation of the instability as compared with the neutral-ion interaction ($\approx \nu_{ino}\delta\underset{\sim}{V}^*_{ai}\cdot\underset{\sim}{V}_n$). Hence, the RHS of (19) can be approximated as

$$\frac{2}{3}k_s^2\left(2\frac{M_e}{M_n}\frac{\nu_{eno}}{\overline{\gamma}_e} + 1\right)\frac{\nu_{ino}}{\overline{\gamma}_i}\delta\underset{\sim}{V}^*_{ai}\cdot\underset{\sim}{V}_n$$

showing that the proposed mechanism depends on the effective ion-neutral coupling. Substituting (17a) into (19) leads to the dispersion relation of the instability, which is a cubic equation of γ (the growth rate), viz.,

$$A\gamma^3 + B\gamma^2 + C\gamma + D = 0 \qquad (20)$$

where

$$A = 1 + \nu_{eno}\nu_{ino}/\Omega_e\Omega_i,$$

$$B = 2(M_e/M_n)\nu_{eno} + \nu_i k_s^2 V_u^2/(\Omega_i^2+\nu_i^2) + \nu_e k_s^2 V_{te}^2/(\Omega_e^2+\nu_e^2)$$
$$+ (10/3)\nu_{eno}k_s^2 V_u^2/\Omega_e\Omega_i,$$

$$C = \nu_{ino}\nu_{eno}\left[k_s^2 V_u^2/(\Omega_i^2+\nu_i^2)\right](2M_e/M_n + k_s^2 V_{te}^2/\Omega_e^2)$$
$$+ (2/3)\nu_{eno}(k_s^2 V_u^2/\Omega_e\Omega_i)\left[10(M_e/M_n)\nu_{eno}\right.$$
$$\left. + 4\nu_{eno}k_s^2 V_{te}^2/\Omega_e^2 + 4\nu_{ino}k_s^2 V_u^2/(\Omega_i^2+\nu_i^2)\right] - (2/3)(k_s^2\nu_{eno}\nu_{ino}/\Omega_e\Omega_i)|V_n|^2,$$

and

$$D = -(2/3)\nu_{ino}\nu_{eno}^2(k_s^2/\Omega_e\Omega_i)(4M_e/M_n + k_s^2 V_{te}^2/\Omega_e^2)|V_n|^2 +$$
$$2\nu_{ino}\nu_{eno}^2(k_s^2 V_u^2/\Omega_e\Omega_i)\left[k_s^2 V_u^2/(\Omega_i^2 + \nu_i^2)\right](2M_e/M_n + k_s^2 V_{te}^2/\Omega_e^2).$$

Although (20) is the dispersion relation derived for the E region case, it can be also applied to the F region when $\underset{\sim}{V}_n \simeq \hat{z}V_{nz}$, namely, when the neutral wind blows primarily along the earth's magnetic field lines.

2.1 The threshold condition

The threshold condition of the instability that is obtained by setting $\gamma = 0$ in the dispersion relation is given by

$$|V_{th}|^2 = \frac{3k_s^2 V_u^4}{(\Omega_i^2 + \nu_i^2)}\left[2\frac{M_e}{M_n} + \frac{k_s^2 V_{te}^2}{\Omega_e^2}\right] \Big/ \left[4\frac{M_e}{M_n} + \frac{k_s^2 V_{te}^2}{\Omega_e^2}\right] \qquad (21)$$

where the two terms, $2M_e/M_n$ and $k_s^2 V_{te}^2/\Omega_e^2$, correspond to the electron cooling due to electron-neutral collisions and the electron cross-field diffusion, respectively. The dormer effect dominates over the latter when the scale lengths ($\lambda_s = 2\pi k_s^{-1}$) of field-aligned ionospheric irregularities exceed $(2\pi V_{te}/\Omega_e)(M_n/2M_e)^{1/2} \sim 8$ meters in the ionospheric E region.

Since $\lambda_s (= 2\pi k_s^{-1})$ is of the order of the gravity wavelength ($\geq$ tens of kilometers), (21) can be approximately written as

$$|V_{th}|^2 \simeq (\frac{3}{2}) \frac{(2\pi V_{ti}^2)^2}{(\Omega_i^2 + \nu_i^2)\lambda_s^2} \simeq \begin{cases} (\frac{3}{2})(\frac{2\pi V_{ti}^2}{\nu_{ino}\lambda_s})^2 & \text{(E region)} \\ (\frac{3}{2})(\frac{2\pi V_{ti}^2}{\Omega_i\lambda_s})^2 & \text{(F region, when } \underset{\sim}{V}_n \simeq \hat{z}V_{nz}\text{).} \end{cases}$$

This expression shows that the threshold condition of the proposed instability is primarily determined by the ion cross-field diffusion damping, whose exact form has been retained. In the ionospheric E region, the ion effective collision frequency (ν_i) is dominantly contributed from the ion-neutral collisions (ν_{ino}) that are much greater than the ion gyro-frequency (Ω_i), that is, $\nu_i \sim \nu_{ino} >> \Omega_i$. This means that ions are essentially unmagnetized and their cross-field diffusion damping is thus identical to their parallel diffusion damping. If we use the following E region parameters (Rishbeth and Garriott, 1969):

$$M(NO^+)/M_e = 5.5 \times 10^4, \Omega_i/2\pi = 25.4 \text{ Hz}, \nu_{ino}(\nu_{eno}) = 5.8 \times 10^3 (9.2 \times 10^4) \text{ Hz}, V_{ti} = 2.54 \times 10^2 \text{m/sec}$$

(or $T_i = 210^0$ K) and $\lambda_s = 100$Km, then $|V_{th}| \sim 8.5 \times 10^{-4}$m/sec. By contrast, $|V_{th}|$ is independent of ν_{ino} in the F region because $\Omega_i >> \nu_{ino}$ in the case that $\underset{\sim}{V}_n \simeq \hat{z}V_{nz}$. This indicates that ions are strongly magnetized and their parallel diffusion damping may greatly exceed their cross-field diffusion damping if the irregularities have a non-zero parallel wave number. With the substitution of

the typical F region parameters:

$M(O^+)/M_e = 2.9 \times 10^4$, $\Omega_i/2\pi = 4.76$Hz, $V_{ti} = 7.6 \times 10^2$ m/sec($T_i = 1000°$K),

and $\lambda_s = 100$Km, the threshold neutral velocity perturbation is 1.5×10^{-1} m/sec that is greater than $|V_{th}|$ in the E region by about two orders of magnitude. But, if the neutral wind blows dominantly across the earth's magnetic field (i.e., $\underset{\sim}{V}_n \simeq \underset{\sim}{V}_{n\perp}$, it can be expected from (17b) that the threshold velocity in the F region is enhanced by another factor of $\Omega_i/\nu_{ino} \sim 400$. In other words, $|V_{th}(\sim 60$m/sec) in the F region exceeds that in the E region by four orders of magnitude. The threshold in the E region seems to be rather small compared with the typical neutral velocity perturbation of gravity waves that is of the order of 40 m/sec. However, a small threshold does not necessarily ensure the growth rate to be large enough for the practical excitation of the instability. As shown later, the proposed instability can be only practically triggered by gravity waves with periods of a few tens of minutes.

2.2 The growth rates

For the excitation of modes with $\lambda_s >> (2\pi V_{te}/\Omega_e)(M_n/2M_e)^{1/2} \sim 8$ (13) meters in the E (F) region, the coefficients of the cubic equation (20) have the following simple form:

$$A \simeq 1 + \nu_{eno}\nu_{ino}/\Omega_e\Omega_i \sim 1.4 \text{ (E region) and } 1.0 \text{ (F region).}$$
$$B \simeq 2(M_e/M_n)\,\nu_{eno} \sim 3.3 \text{ (E region) and } 4.1 \times 10^{-4} \text{ (F region),}$$

$$C \simeq 2\nu_{eno}(k_s^2 V_{ti}^2/\nu_{ino})(M_e/M_n)[1 - (1/3)(\nu_{ino}/\Omega_i)^2(V_n/V_{ti})^2]$$
$$\sim 1.42 \times 10^{-5} \text{(E region) and } 1.0 \times 10^{-6} \text{ (F region),}$$

$$D \sim 4(k_s V_{te}\nu_{eno}/\Omega_e)^2(k_s^2 V_{ti}^2/\nu_{ino})(M_e/M_n)[1 - (V_n/V_{th})^2]$$
$$\sim -1.48 \times 10^{-5} \text{ (E region) and } -1.86 \times 10^{-12} \text{ (F region),}$$

for $V_n = 40$m/sec, $\lambda_s = 100$ Km, $\nu_{ino} = 5.8 \times 10^3$ Hz(0.5Hz), and $\nu_{eno} = 9.2 \times 10^4$ Hz (12 Hz), in the E (F) region. Therefore, instead of solving the cubic

equation, γ can be derived approximately from

$$2\left(\frac{M_e}{M_n}\right)\nu_{eno}\gamma^2 \simeq 4\frac{k_s^2 V_{te}^2 \nu_{eno}^2}{\Omega_e^2}\frac{k_s^2 V_{ti}^2}{\nu_{ino}}\left(\frac{M_e}{M_n}\right)\left[\left(\frac{V_n}{V_{th}}\right)^2 - 1\right] \qquad (23)$$

where V_{th} is given by (22). Since $V_n \gg V_{th}$, Equation (23) can be written as

$$\gamma \simeq \begin{cases} \frac{4\pi}{\sqrt{3}}\frac{V_n}{\lambda_s}\left(\frac{\nu_{eno}\nu_{ino}}{\Omega_e\Omega_i}\right)^{1/2} \sim 2.0 \times 10^{-3}\ \text{sec}^{-1} & \text{(E region)} \\ \frac{4\pi}{\sqrt{3}}\frac{V_n}{\lambda_s}\left(\frac{\Omega_i\nu_{eno}}{\Omega_e\nu_{ino}}\right)^{1/2} \sim 6.0 \times 10^{-5}\ \text{sec}^{-1} & \text{(F region, when } \underset{\sim}{V}_n \simeq \hat{z}V_{nz}\text{)} \end{cases}$$

for $\lambda_s = 100$ Km. It is apparent that the neutral-plasma interaction is much more effective in the E region than in the F region. The growth rate is inversely proportional to the scale length of field-aligned ionospheric irregularities that is of the order of the neutral wave wavelength. While a maximum scale length of 400 Km was detected by ALTAIR from the horizontal wave structure, the nighttime ionosphere spatially modulated with shorter scale lengths ($\sim$35 Km) prior to the onset of ESF was sensed by the amplitude scintillations of gesostationary satellite signals at 136 (MHz) (J.A. Klobuchar, private communication, (1984). The growth rate in the E region for $\lambda_s = 35$Km is 6.0×10^{-3} sec^{-1} in this situation. Since the wavelengths of neutral waves are tens of kilometers or longer, the instability is expected to have 10^{-2} sec^{-1} as the upper bound of its growth rate in the ionospheric E region. The growth rates have to exceed the molecular ion recombination rate ($\sim 10^{-3}$ sec^{-1}) for the operation of the instability.

In the formulation of the theory, $R_e(\omega_a) \gtrsim \gamma$ has been assumed, where ω_a is the angular frequency of the forced ion acoustic mode. The real angular frequency, $R_e(\omega_a)$, is essentially equal to the neutral wave frequency (ω_o) because of the excitation of ionospheric irregularities as nearly zero-frequency modes.

This condition requires that the neutral wave frequency (ω_o) be greater than $\gamma \sim 2.0 \times 10^{-3}$ Hz, namely, the neutral waves have periods ($T_o = 2\pi/\omega_o$) less than one hour. A clear portrait of the neutral pump waves can be delineated at this point: they are characterized with short periods (< one hour) and wavelengths of tens to hundreds of kilometers.

0.30 Seeding the ESF

The neutral wave-plasma interaction, as shown above, is not effective enough for the excitation of large-scale ionospheric irregularities in the F region. One may note, however, from (24) that in the F region, $\gamma \propto \nu_{ino}^{-1/2}$ and argue that smaller ν_{ino} at higher altitudes can lead to a larger growth rate. Two other things should also be noted: (1) ν_{ino} cannot be too small because $\nu_{ino} \gg \gamma$ has been assumed in the formulation of the theory, and (2) $\gamma \propto \nu_{eno}^{1/2}$ and ν_{eno} is smaller at higher altitudes. Actually, $\nu_{eno}/\nu_{ino} \leq 10^2$ at any altitude in the ionosphere. Hence, even if we take $\nu_{eno}/\nu_{ino} = 10^2$, the growth rate is 5.2×10^{-4} sec^{-1} for $\lambda_s = 35$ Km in the case that the neutral wind blows along the earth's magnetic field. This growth rate can exceed the atomic ion recombination rate above a certain height. Nevertheless, if the neutral wind blows dominantly across the earth's magnetic field, the growth rate in the F region is reduced by at least two orders of magnitude. Moreover, the conditions for the instability become extremely stringent when the parallel heat conduction loss in the F region is not negligible. This effect can largely raise the threshold and decrease the growth rate of the instability. The excitation of the instability with a rather small growth rate requires almost a continuous source of neutral waves.

While the forced ion acoustic modes are highly damped in the E region, the concurrently excited large-scale ionospheric irregularities have much less diffusion damping and can survive for hours after the disappearance of the

neutral-wave source(s). The electric field perturbations associated with the large-scale E region irregularities can extend along the geomagnetic field and many onto the F region (Farley 1960). These intense electric field perturbations then seed the F region for the subsequent excitation of the Rayleigh-Taylor instability that has been generally accepted to be the cause for the spread F echoes on the ionograms and the plumes on the VHF backscatter radar maps.

IV. Summary

The data measured by the Dynamics Explorer 2 spacecraft (DE-2) provide a unique opportunity to determine many geographical parameters. In this report we present the results of analyses on two sets of data measured in two different days. On comparing the data, it is seen that there is a lasting effect of previous magnetic activity on the fluctuations for day 81288 in that the fluctuations are about double those for day 81248. This doubling is consistent with the Joule heating for the two days. The power spectra are also in agreement with this ratio. The ratio of powers being the square of the fluctuation amplitude is found to be about 5.7 for oxygen and 4.0 for nitrogen. Our analyses appear to favor Joule heating as the driver of observed wavelike fluctuations in neutrals rather than precipitation. It may be that the neutrals are excited by the entire auroral oval in the Joule heating pulse and filtering yields wavelike, rather than irregular, variation. Ion waves are then excited by the neutral waves through the ion-neutral collisional coupling.

A theoretical model exploring the role of neutral waves on the generation of large scale plasma density irregularities is also presented. This model is preliminary in the sense that equational latitude is considered so that the effect of anistropy introduced by the geomagnetic fleid on plasma motion is minimized. This simplifies the analysis a great deal. Nevertheless, the results of the analysis can be applied to explain the the equatorial spread F (ESF) phenomenon. The neutral waves of interest are characterized by wavelengths of tens to a few hundreds of kilometers and by periods of a few tens of minutes. The efficient excitation of ionospheric irregularities by our proposed mechanism relies on large plasma-neutral collisions. Such an optimum environment can be provided by the E region rather than the F region. Since neutral waves interact primarily with ions, the threshold of the instability is

determined by the ion heat conduction loss. It is shown that the plasma irregularities can be generated within a few minutes when large amplitude gravity waves are present.

REFERENCES

Anderson, D. N. and G. Haerendel, The motion of depleted plasma regions in the equatorial ionosphere, J. Geophys. Res., 84, 4251, 1979.

Anderson, D. N., A. D. Richmond, B. Balsley, R. G. Roble, M. A. Biondi and D. F. Sipler, In-situ generated gravity waves as a possible seeding mechanism for equatorial spread-F. Geophys. Rev. Lett. 9, 789-792, 1982.

Baker, D. M. and K. Davies, F2-region acoustic waves from severe weather. J. Atmos. Terr. Phys. 31, 1345-1352, 1969.

Balsley, B. B., G. Haerendel, and R. A. Greenwald, Equatorial spread F: recent observations and a new interpretation, J. Geophys. Res., 77, 5625, 1972.

Beer, T., Spatial resonance in the ionosphere, Planet. Space Sci., 21, 297, 1973a.

Beer, T., Supersonic generation of atmospheric waves, Nature, 242, 34, 1973b.

Bertin, F., J. Testud, L. Kerskey and P. R. Rees, The meteorological jet stream as a source of medium scale gravity waves in the thermosphere; an experimental study. J. Atmos. Terr. Phys. 40, 1161-1183, 1978.

Booker, H. G. and H. W. Wells, Scattering of radio waves by the F-region of ionosphere, Terres. Mag., 43, 249, 1938.

Booker, H. G., The role of acoustic gravity waves in generation of spread-F and ionospheric scintillation, J. Atmos. Terr. Phys., 41, 501, 1979.

Bowman, G. G. and K. L. Shrestha, Ionospheric storms and small pressure fluctuations at ground level. Nature 210, 1032-1034, 1966.

Chandra, S. and J. R. Herman, F-region ionization and heating during magnetic storms. Planet. Space Sci. 17, 841-851, 1969.

Chandra, S. and N. W. Spencer, Exospheric temperature inferred from the Aeros-A neutral composition measurement. J. Geophys. Res. 80, 3615-3621, 1975.

Chandra, S. and N. W. Spencer, Thermospheric storms and related ionospheric effects. J. Geophys. Res. 81, 5018-5026, 1976.

Chimonas, G. and C. O. Hines, Atmospheric gravity waves launched by auroral currents. Planet. Space Sci. 18, 565-582, 1970.

Chimonas, G. and W. R. Peltier, The bow wave generated by an auroral arc in supersonic motion. Planet. Space Sc. 18, 599-612, 1970.

Chimonas, G. and W. R. Peltier, On severe storm acoustic signals observed at ionospheric heights. J. Atmos. Terr. Phys. 36, 821-828, 1974.

Ching, B. K. and Y. T. Chiu, Global distribution of the thermospheric heat sources: EUV absorption and Joule dissipation. Planet. Space Sci. 21, 1633-1646, 1973.

Chiu, Y. T. and J. M. Strauss, Rayleigh-Taylor and wind driven instabilities of the nighttime equatorial ionosphere, J. Geophys. Res., 84, 3283, 1979.

Cole, K. D., Electrodynamic heating and movement of the thermosphere. Plant. Space Sci. 19, 59-75, 1971.

Davies, K. and J. E. Jones, Ionospheric disturbances in the F2-region associated with severe thunderstorms. J. Atmos. Sci. 28, 254-262, 1971.

Davis, M. J., On polar substorms as the source of large-scale traveling ionospheric disturbances. J. Geophys. Res. 76, 4525-4533, 1971.

Davis, M. J. and A. V. daRosa, Traveling ionospheric disturbances originating in the auroral oval during polar substorms. J. Geophys. Res. 74, 5721-5735, 1969.

Del Genio, A. D., G. Schubert and J. M. Strauss, Characteristics of acoustic-gravity wave in a diffusively separated atmosphere, J. Geophys. Res. 84, 1865-1879, 1979.

Dudis, J. J. and C. A. Reber, Composition effects in thermospheric gravity waves. Geophys. Res. Lett. 3, 727-730, 1976.

Dungey, J. W., Convective diffusion in the equatorial F-region, J. Atmos. Terr. Phys., 9, 304, 1958.

Dyson, P. L., C. P. Newton and L. H. Brace, In situ measurements of neutral and electron density wave structure from the Explorer 32 satellite. J. Geophys. Res. 75, 3200-3210, 1970.

Eun, H. and S. H. Gross, Ionospheric disturbances and gravity waves. J. Geophys. Res. 81, 3261-3270, 1976a.

Farley, D. T., A theory of electrostatic fields in the ionosphere at nonpolar geomagnetic latitudes, J. Geophys. Res., 65, 869, 1960.

Fraser, G. J. and M. R. Thorpe, Experimental investigation of ionospheric/stratospheric coupling in southern mid-latitudes-1. Spectra and cross-

spectra of stratospheric temperatures and the ionospheric f-min parameter. J. Atmos. Terr. Phys. 38, 1003-1011, 1976a.

Fraser, G. J. and M. R. Thorpe, Experimental investigation of ionospheric/stratospheric coupling in southern mid-latitudes -2. Comparison of mesospheric electron densities and drifts with stratospheric temperatures and winds. J. Atmos. Terr. Phys. 38, 1013-1016, 1976b

Georges, T. M., HF doppler studies of traveling ionospheric disturbances. J. Atmos. Terr. Phys. 30, 735-746, 1968.

Glass, M. and A. Spizzichino, Waves in the lower thermosphere: Recent experimental investigations. J. Atmos. Terr. Phys. 36, 1825-1839, 1974.

Gross, S. H., Model analysis of large scale wave structure as observed by AE satellites, Paper SA100, Spring meeting of the American Geophysical Union, May 22-27, Toronto, Canada, EOS 61, 322-323, 1980.

Gross, S. H., Global large scale structures in the F region, submitted to J. Geophys. Res., 1984.

Gross, S. H. and H. Eun, Traveling neutral disturbances, Geophys. Res. Lett. 3, 257-260, 1976.

Gross, S. H. and H. Eun, Traveling neutral disturbances and minor constituent particle mass. J. Atm. Terr. Phys. 40, 183-193, 1978.

Gross, S. H. and F. Huang, Medium scale waves in the thermosphere observed by the AE-C satellite, to be published in IEEE Trans. on Geoscience and Remdote Sensing, 1984.

Gross, S. H., C. A. Reber and F. Huang, Large scale waves in the ionosphere

observed by the AE satellites, AGARD meeting, Pozzuoli, Italy, Oct. 21-27, in AGARD Conference Proceedings No. 295, The physical basis of the ionosphere in the solar-terrestrial system, 27th meeting of the Electromagnetic Wave Propagation Panel, 1980.

Gross, S. H., C. A. Reber and F. Huang, Large scale structures observed in the thermosphere, Paper SA-26, Spring meeting of the American Geophysical Union, May 25-29, Baltimore, Maryland, 1981a.

Gross, S. H., C. A. Reber and F. Huang, Large scale waves in the ionosphere at equatorial latitudes, XXth General Assembly of URSI, 11-18 August, Washington, D.C., 1981b.

Gross, S. H., C. A. Reber and F. Huang, Gravity waves in the thermosphere observed by the AE satellites, POLY MRI Report No. 1426-82, 1982.

Gross, S. H., C. A. Reber and F. Huang, Large scale waves in the thermosphere observed by the AE-C satellite, IEEE Trans. on Geoscience and Remote Sensing, pp. 340-352, July 1984, (see attached paper).

Haerendel, G. Theory of equatorial spread F, Max-Planck-Institute für Physik and Astrophysik, Institute für Physik and Astrophysik, Institut für terrestrisches Physik, Garching, West Germany, 1973.

Hays, P.B., R. A. Jones and M. H. Rees, Auroral heating and the composition of the neutral atmosphere. Planet. Space Sci. 21, 559-573, 1973.

Hedin, A. E. , J.E. Salah, J. V. Evans, C. A. Reber, G. P. Newton, N. W. Spencer, D. C. Kayer, D. Alcayde, P. Bauer, L. Coggerand, J.P. McClure, A global thermospheric model based on mass spectrometer and incoherent scatter data, MSIS 1·N_2 density and temperature. J.

Geophys. Res. 82, 2130-2147, 1977.

Herman, J. R., Spread F and ionsopheric F-region irregularities, Rev. Geophys., 4, 255, 1966.

Herron, T. J. and H. Montes, Correlation of atmospheric pressure waves with ionospheric doppler signals. J. atmos. Sci. 27, 51-54 1970.

Hines, C.O., International atmospheric gravity waves at ionospheric heights, Canadian J. Phys., 38, 1441, 1960.

Hines, C.O., Dynamic heating of the upper atmosphere. J. Geophys. Res. 70, 177-183, 1965.

Hines, C.O., Tidal oscillations, shorter period gravity waves and shear waves, Meterological Monographs, 9, 114, 1968.

Hines, C.O., Generalizations of the Richardson criterion for the onset of atmospheric turbulence, Quart. Journ. of the Royal Meterological Soc., 97, 429, 1971.

Hines, The upper atmosphere in motion. Geophysical Monograph 18, American Geophysical Union, Washington, D.C., 1974.

Hoegy, W.R., L. H. Brace, A.E. Hedin, G. R. Carignan, Gravity waves and TID's observed on Dynamic Explorer, EOS 62, 997 (1981).

Hoegy, W. R., L. H. Brace, A. E. Hedin, G. R. Carignan, DE observations of gravity waves and traveling ionospheric disturbances at mid-to-high-latitudes, manuscript in preparation, 1983.

Huang, F., C.A. Reber and S.H. Gross, Large scale waves in the atmosphere

and ionosphere observed by the AE satellites, Paper SA 101, Spring meeting of The American Geophysical Union, May 22-27, Toronto, Canada, EOS 61, 323, 1980.

Hudson, M.D. and C.F. Kennel, Linear theory of equatorial spread F, J. Geophys. Res., 80, 4581, 1975. Hunsucker, R.D., Atmospheric gravity waves generated in the high latitude ionosphere. Rev. Geophys. Sp. Phys. 20, 293-315, 1982.

Hunsucker, R.D., Private communication, 1983.

Jacchia, L.G., J. Slowey and F. Veriani, Geomagnetic perturbations and upper atmospheric heating. J. Geophys. Res. 72, 1423-1434, 1967.

Kelley, M.C., M.F. Larsen, C. LaHoz and J.P. McClure, Gravity wave initiation of equatorial spread F: A case study. J. Geophys. Res. 86, 9087-9100, 1981.

Khan, M.S.H., Sporadic E. structures and pressure oscillations at ground level. Aust. J. Phys. 23, 719-30, 1970.

Klostermeyer, J., Gravity waves in the F-region. J. Atmos. Terr. Phys. 31, 25-45, 1969.

Klostermeyer, J., Thermospheric heating by atmospheric gravity waves. J. Atmos. Terr. phys. 2267-2275, 1973.

Klostermeyer, J., Nonlinear investigation of the spatial resonance effect in the nighttime equatorial F region, J. Geophys. Res., 83, 3753, 1978.

Larsen, M.F., W.E. Swartz, R.F. Woodman, Gravity wave generation by thunderstorms observed with a vertically-pointing 430 MHz radar.

Geophys. Res. Lett. 9, 571-574, 1982.

Lindzen, R.S. and D. Blake, Mean heating of the thermosphere by tides JGR 75, 6868-6871, 1970.

Lui, A.T.Y., C. - I. Meng and S. Ismail, Large amplitude undulation on the equatorial boundary of the diffuse aurora, J. Geophys. Res. 87, 2385-2400, 1982.

Manson, A.H., Coupling effects between the ionosphere and stratosphere in Canada (45°, 75°W), 1962-1966. J. Atmos. Terr. Phys. 30, 627-632, 1968.

Manson, A.H., Stratospheric-ionospheric-magnetospheric coupling at mid-latitudes in the southern hemisphere, 1969-74. J. Atmos. Terr. Phys. 38, 1017-1020, 1976.

Mastrantonio, G., F. Einaudi, D. Fua and D.P. Lalas, Generation of gravity waves by Jet Streams in the atmosphere. J. Atmos. Sci. 33, 1730-1738, 1976.

Mayr, H.G., I. Harris, F.A. Herrero and F. Varosi, Global excitation and propagation of gravity waves in a dissipative multi-constituent medium. Paper SA 42A-08, EOS 63, 1051, 1982.

Mayr, H.G., I. Harris, F.A. Herrero and F. Variosi, Global excitation and propagation of gravity waves in a dissipative multi-constitutent medium: 1. Transfer function, paper in preparation, 1983.

Mayr, H.G., I. Harris and N.W. Spencer, Some properties of upper atmosphere dynamics. Rev. Geophys. Space Phys. 16, 539-565, 1978.

Mayr, G.H. and H. Volland, Magnetic storm effects in the neutral composition. Planet. 20, 379-393, 1972.

Mayr, G.H. and H. Volland, Magnetic storm characteristics of the thermosphere. J. Geophys. Res. 78, 2251-2264, 1973.

Mayr, H.C. and H. Volland, Magnetic storm dynamics of the thermosphere, J. Atmos. Terr. Phys. 36, 2025-2036, 1974.

Mayr, H.G. and H. Volland, Composition waves in the thermosphere, J. Geophysics Res., 671-676, 1976.

Morgan, M.G., Locating TID sources with a north-south chain rapid-run ionosondes in Western Quebec, in print, Radio Science, 1983.

Morgan M.G., C.H. J. Calderon, and K.A. Ballard, Techniques for the study of TID's with multi-station rapid-run ionosondes, Radio Sci. 13, 729-741, 1978.

Morgan, M.G. and B.L. Tedd, The dispersion of traveling ionospheric disturbances, to be published in J. Geophys. Res., 1983.

Ossakow, S.L., Ionospheric irregularities, Rev. Geophys. Space Phys., 17, 521, 1979.

Potter, W.E., D.C. Kayser and K. Mauersberger, Direct measurements of neutral wave characteristics in the thermosphere. J. Geophys. res. 81, 5002-5012, 1976.

Prasad, S.S., L.J. Schneck and K. Davies, Ionospheric disturbances by severe tropospheric weather storms. J. Atmos. Terr. Phys. 37, 1357-1363, 1975.

Prolss, G.W. Perturbation of the low-latitude upper atmosphere during magnetic storm activity, J. Geophys. Res. 87, 5260-5266, 1982.

Prolss, G.W. and U. von Zahn, Magnetic storm associated changes in neutral composition of the atmosphere at mid-latitudes observed by the ESRO 4 gas analyzer. Space Research XIV, Akademie-Verlag, Berlin, 1974, pp. 157-161, 1974a.

Prolss, G.W. and U. von Zahn, ESRO 4 gas analyzer results 2. Direct measurements of changes in the neutral composition during an ionospheric storm. J. Geophys. Res. 79, 2535-2539, 1974b.

Rastogi, R.G. and R.F. Woodman, Spread F in equatorial ionograms associated with reversal of horizontal F region electric field, Ann. Geophys., 34, 31, 1978.

Reber, C.A. and A.E. Hedin, Heating of the high-latitude thermosphere during magnetically quiet periods. J. Geophys. Res. 79, 2457-2461, 1974.

Reber, C.A., A.E. Hedin, D.T. Pelz, N.E. Potter and L.H. Brace, Phase and amplitude relationships of wave structure observed in the lower thermosphere. J. Geophys. Res. 80, 4576-4580, 1975.

Richmond, A.E., Thermopheric heating in a magnetic storm: Dynamic transport of energy from high to low latitudes. J. Geophys. Res. 84, 5259-5266, 1979.

Richmond, A.E. and S. Matsushita, Thermospheric response to a magnetic substorm. J. Geophys. Res. 80, 2839-2850, 1975.

Richmond, A.D. and R.G. Roble, Dynamic effects of aurora-generated gravity

waves on the mid-latitude ionosphere. J. Atmos. Terr. Phys. 41, 841-852, 1979.

Rishbeth H. and O.K. Garriott, Introduction to ionospheric physics, Academic Press, New York, 1969.

Rishbeth H., Polarization fields produced by winds in the equatorial F-region, Planet. Space Sci., 19, 357, 1971.

Roble, R.G., A.D. Richmond, W.L. Oliver and R.M. Harper, Ionospheric effects of the gravity wave launched by the September 18, 1974, sudden commencement. J. Geophys. Res. 83, 999-1009, 1978.

Roemer, M., Geomagnetic activity effect on atmospheric density in the 250 to 800 km altitude region. Space Research XI, 965-974, 1971.

Röttger, J., Wave-like structures of large-scale equatorial spread-F irregularities, J. Atmos. Terr. Phys., 35, 1195, 1973.

Röttger, J., The macro-scale structure of equatorial spread F irregularities, J. Atmos. Terr. Phys., 35, 1195, 1973.

Röttger, J., Drifting patches of equatorial spread-F irregularities- experimental support for the spatial resonance mechanism in the ionosphere, J. Atmos. Terr. Phys., 40, 1103, 1978.

Scannapieco, A.J. and S.L. Ossakow, Nonlinear equatorial spread F, Geophys. Res. Lett., 3, 451, 1976.

Shrestha, K.L., Anomalous ionospheric absorption and microbarometric activity at ground level. J. Atmos. Terr. Phys. 33, 213-219, 1971a.

Shrestha, K.L., Sporadic-E and atmospheric pressure waves. J. Atmos. Terr. Phys. 33, 205-211, 1971b.

Taeusch, D.R., G.R. Carignan and C.A. Reber, Neutral composition variation above 400 kilometers during a magnetic storm. J. Geophys. Res. 76, 8318-8325, 1971.

Testud, J., Gravity waves generated during magnetic substorms. J. Atmos. Terr. Phys. 32, 1793-1805, 1970.

Testud, J., P. Amayenc and M. Blanc, Middle and low latitude effects of auroral disturbances from incoherent scatter. J. Atmos. Terr. Phys. 37, 898-1009, 1975.

Thome, G., Long-period waves generated in the polar ionosphere during the onset of magnetic storms. J. Geophys. Res. 73, 6319-6336, 1968.

Towle, D.M., VHF and UHF radar observations of equatorial F-region ionospheric irregularities and background densities, Radio Sci., 15, 71, 1980.

Trinks, H., K.H. Fricke, U. Laux, G.W. Prolss and U. von Zahn, ESRO 4 gas analyzer results 3. Spatial and temporal structure of the mid-latitude atmosphere during a geomagnectic storm. J. Geophys. Res. 80, 4571-4575, 1975.

Trinks, H. S. Chandra, N.W. Spencer and U. von Zahan, A two satellite study of the neutral atmosphere response to a major geomagnetic storm. J. Geophys. Res. 81, 5013-5017, 1976.

Trinks, H. and H.G. Mayr, Large-scale neutral composition gravity waves in the thermosphere observed by ESRO 4. J. Geophys. Res. 81, 4023-4026,

1976.

Vickrey, J.F., R. R. Vondrak and S.J. Mathews, Energy deposition by precipitating particles and Joule dissipation in the auroral ionosphere. J. Geophys Res. 87, 5184-5196, 1982.

Tsunoda, R.T., M.J. Baron, J. Owen, and D.M. Towle, ALTAIR: an incoherent scatter radar for equatorial spread-F studies, Radio Sci., 14, 1111, 1979.

Tsunoda, R.T., Backscatter measurements of 11-cm equatorial spread-F irregularities, Geophys. Res. Lett., 7, 848, 1980a.

Tsunoda, R.T., Magnetic-field-aligned characteristics of plasma bubbles in the nighttime equatorial ionosphere, J. Atmos. Terr. Phys., 42, 743, 1980b.

Tsunoda, R.T. and B.R. White, On the generation and growth of equatorial backscatter plumes, 1, Wave structure in the bottomside F layer, J. Geophys. Res., 86, 3610, 1981.

Tsunoda, R.T., R.C. Livingston and C.L. Rino, Evidence of a velocity shear in bulk plasma motion associated with the post-sunset rise of the equatorial F layer, Geophys. Res. Lett., 8, 807, 1981.

Tsunoda, T.T., R.C. Livingston, J.P. McClure, and W.B. Hanson, Equatorial plasma bubbles: vertically elongated wedges from the bottomside F layer, J. Geophys. Res., 87, 9171, 1982.

Tsunoda, R.T., R.D. Hake, M.A. Biondo, and D.P. Sipler, On the generation and growth of equatorial backscatter plumes, 3. The roles of neutral wind, waves and velocity shear, J. Geophys. Res., 1984, submitted.

Weber, E.J., J. Buchau, R.H. Eather and S.B. Mende, North-south aligned equatorial airglow depletions, J. Geophys. Res., 83, 712, 1978.

Wickwar, V.B., M.J. Baron and R.D. Sears, Auroral energy input from energetic electrons and Joule heating at Chatanika. J. Geophys. Res. 80, 4364-4367, 1975.

Whitehead, J.D., Ionization disturbances caused by gravity waves in the presence of an electrostatic field and background wind, J. Geophys. Res., 76, 238, 1971.

Yeh, K.C. and C.H. Liu, Acoustic-gravity waves in the upper atmosphere. Rev. Geophys. Space Phys. 12, 193-216, 1974.

Fig. 1 Polar plots of the orbital passes for September 5, 1981, day 81248, orbit number 492 and for October 15, 1981, day 81288, orbit number 1071. The plot is invariant latitude vs magnetic local time.

Fig. 2 Plots of electron precipitation (toppanel), electric field turbulence (second panel) 8-16 Hz as dots and 4-16 kHz as the letter O, electron temperature (middle panel), ion density (fourth panel) and horizontal (H) and vertical (V) winds vs time in hours and minutes UT, invariant latitude, magnetic local time, altitude, local solar time, latitude and longitude. This figure is for orbit 492 on day 81248 for the twelve minutes from 21:10 to 21:22.

Fig. 3 Plots of electron precipitation (top panel), electric field turbulence (second panel) 8-16 HZ as dots and 4-16 kHz as the letter 0, electron temperature (middle panel), ion density (fourth panel) and horizontal (H) and vertical (V) winds vs time in hours and minutes UT, invariant latitude, magnetic local time, altitude local solar time, latitude and longitude. This figure is for orbit 1071 on day 81288 for the twelve minutes from 21:10 to 21:22.

Fig. 4 Graphs for day 81248 on the left and day 81288 on the right. Each graph contains plots of the measured variation in the x, y, z components of the magnetic field relative to a Magsat model ΔBX, ΔBY , ΔBZ , the x component of the electric field EX and the integrated downward Joule heating flux SY vs time in hours and minutes UT for each day. x is along the velocity vector of the spacecraft, y is upward and z is eastward or westward according to the spacecraft direction, north or south. The plot SY has been plotted as positive to mean downward, opposite that of the y axis.

Fig. 5 Graphs of the densities of oxygen, nitrogen and ions and the electron temperature vs time in seconds UT as well as hours, minutes and seconds UT, shown above each graph. Also given are scales for altitude, latitude, longitude, solar zenith angle, local magnetic time and invariant latitude in each graph. The density scales in particules/cm^3 are logarithmic and on the left and the temperature scale in ^{o}K is linear and on the right. The upper graph is for 81248. The lower for 81288.

Fig. 6 Plots of fluctuations obtained by passing the logarithm of the ion, oxygen and nitrogen densities through a bandpass filter that passes structures with scale sizes from 90 to 1500 km. The plots are vs time in seconds UT. The data are for orbit 492 on day 81248.

Fig. 7 FFT spectra of the fluctuations in Figure 6 for day 81248. The spectra are plotted vs period in seconds.

Fig. 8 Plots of fluctuations obtained by passing the logarithm of the ion, oxygen and nitrogen densities through a bandpass filter that passes structures with scale sizes from 90 to 1500 km. The plots are vs time in seconds UT. The data are for orbit 492 on day 81288.

Fig. 9 Plots of fluctuations obtained by passing the logarithm of the ion, oxygen and nitrogen densities through a bandpass filter that passes structures with scale sizes from 90 to 1500 km. The plots are vs time in seconds UT. The data are for orbit 492 on day 81288.

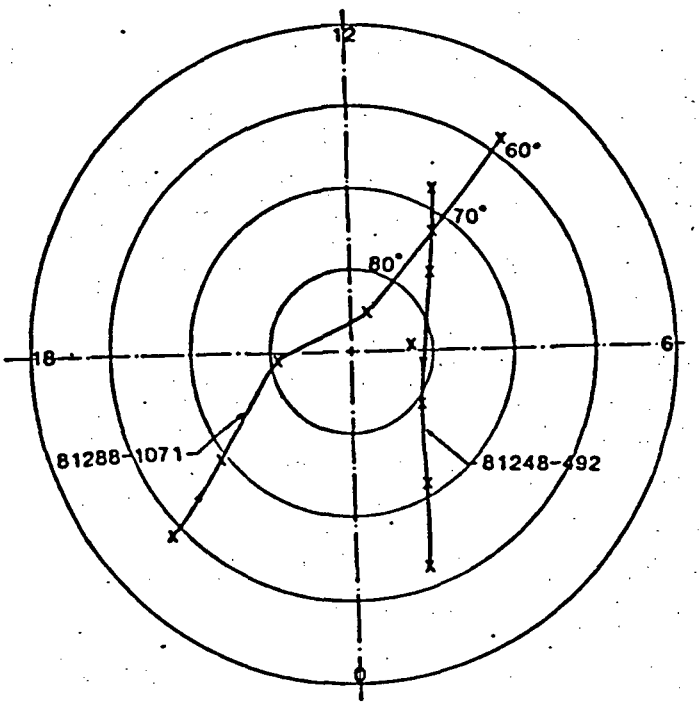

Fig. 1 Polar plots of the orbital passes for September 5, 1981, day 81248, orbit number 492 and for October 15, 1981, day 81288, orbit number 1071. The plot is invariant latitude vs magnetic local time.

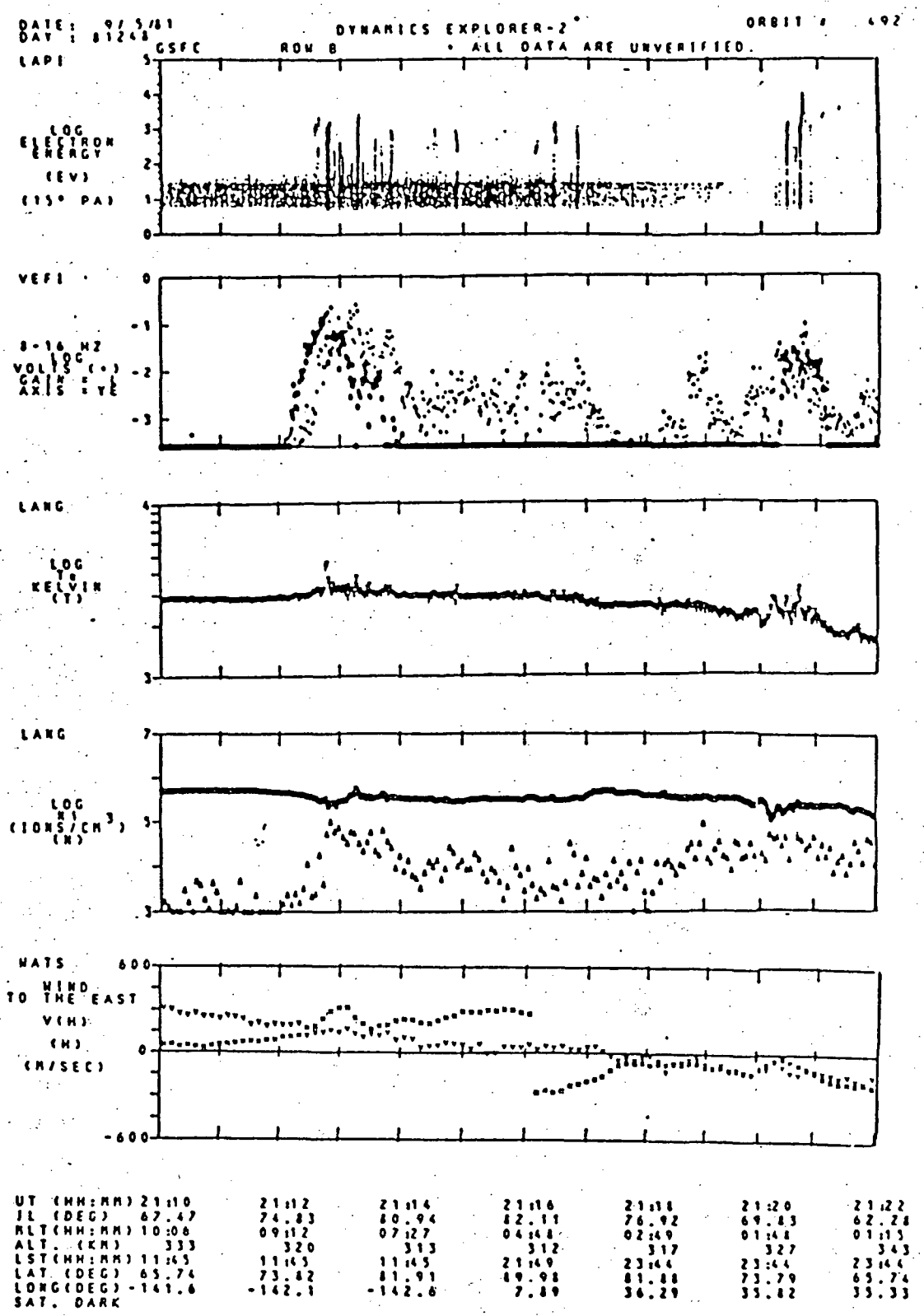

Fig. 2. Plots of electron precipitation (top panel), electric field turbulence (second panel) 8-16 Hz as dots and 4-16 kHz as the letter 0, electron temperature (middle panel), ion density (fourth panel) and horizontal (H) and vertical (V) winds vs time in hours and minutes UT, invariant latitude, magnetic local time, altitude, local solar time, latitude and longitude. This figure is for orbit 492 on day 81248 for the twelve minutes from 21: 10 to 21: 22.

ORIGINAL PAGE IS OF POOR QUALITY

ORIGINAL PAGE IS
OF POOR QUALITY

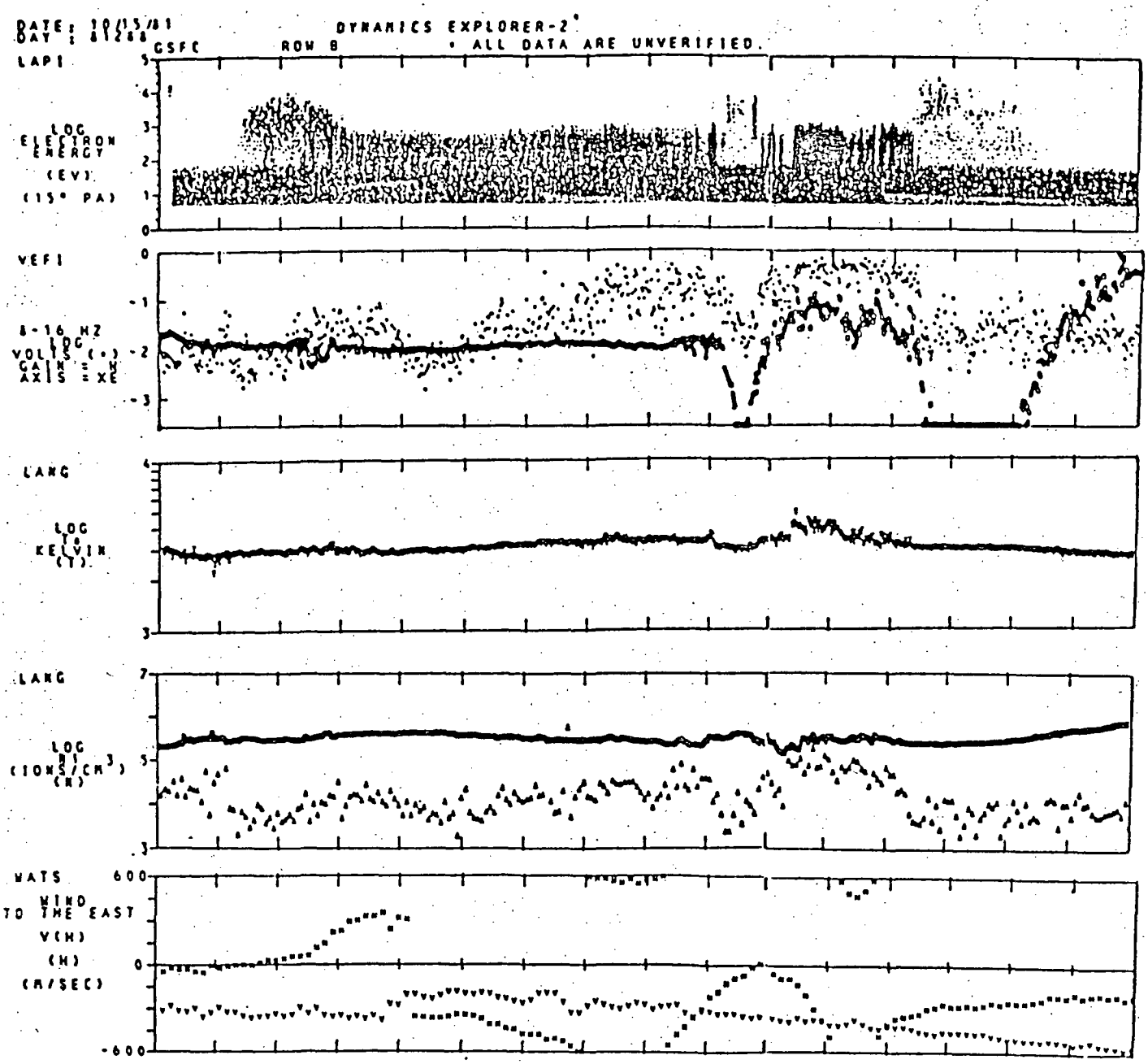

UT (HH:MM)	00:40	00:42	00:44	00:46	00:48	00:50	00:52	00:54	00:56
IL (DEG)	58.44	65.36	72.64	80.20	999.00	83.88	75.55	66.92	58.07
MLT(HH:MM)	20:51	20:42	20:24	19:21	12:22	10:10	09:44	09:33	09:27
ALT. (KM)	456	424	396	372	352	336	325	320	320
LST(HH:MM)	21:23	21:23	21:24	09:22	09:22	09:22	09:22	09:22	09:22
LAT (DEG)	-72.20	-80.00	-87.86	-84.22	-76.24	-68.22	-60.15	-52.06	-43.96
LONG(DEG)	-52.72	-53.18	-53.30	125.54	125.14	124.67	124.18	123.69	123.19
SAT.	DARK								

g. 3. The same as Figure 2, but for orbit 1071 on day 81288.

81248-492

81288-1071

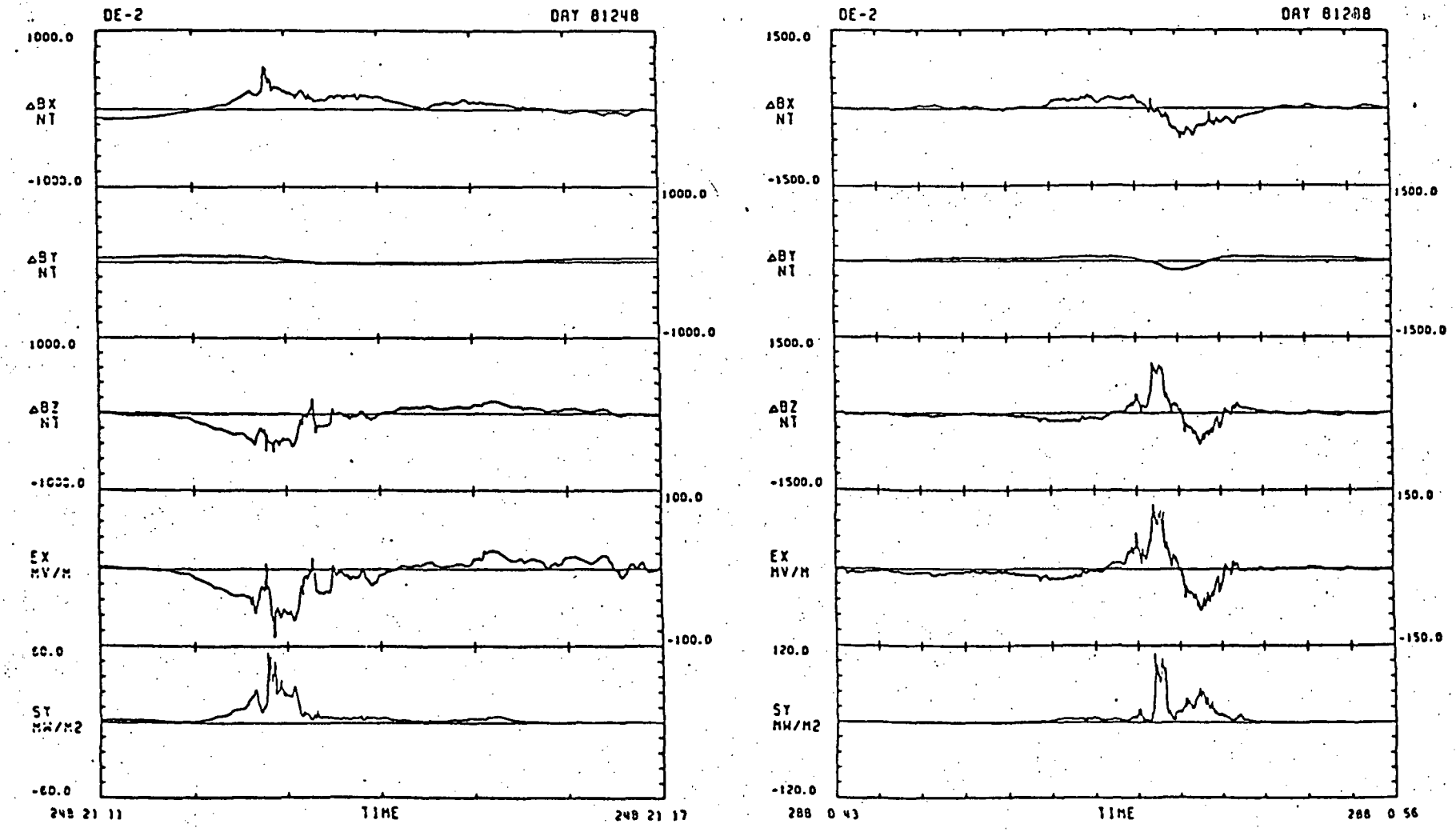

Fig. 4. Graphs for day 81248 on the left and day 81288 on the right. Each graph contains plots of the measured variation in the x, y, z components of the magnetic field relative to a Magsat model ΔBX, ΔBY, ΔBZ, the x component of the electric field EX and the integrated downward Joule heating flux SY vs time in hours and minutes UT for each day. x is along the velocity vector of the spacecraft, y is upward and z is eastward or westward according to the spacecraft direction, north or south. The plot SY has been plotted as positive to mean downward, opposite that of the y axis.

ORIGINAL PAGE IS
OF POOR QUALITY

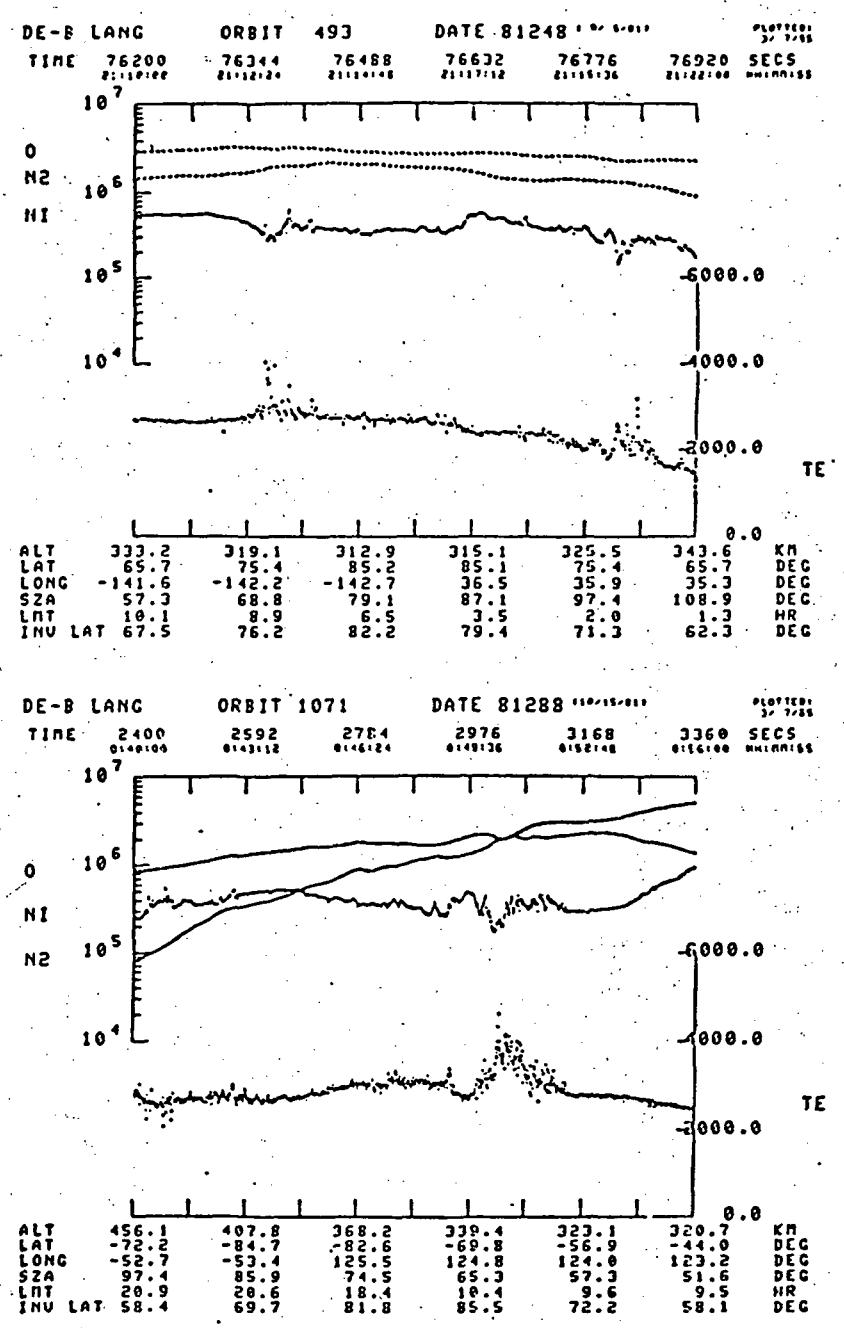

Fig. 5. Graphs of the densities of oxygen, nitrogen and ions and the electron temperature vs time in seconds UT as well as hours, minutes and seconds UT, shown above each graph. Also given are scales for altitude, latitude, longitude, solar zenith angle, local magnetic time and invariant latitude in each graph. The density scales in particles/cm^3 are logarithmic and on the left and the temperature scale in ^{o}K is linear and on the right. The upper graph is for 81248. The lower for 81288.

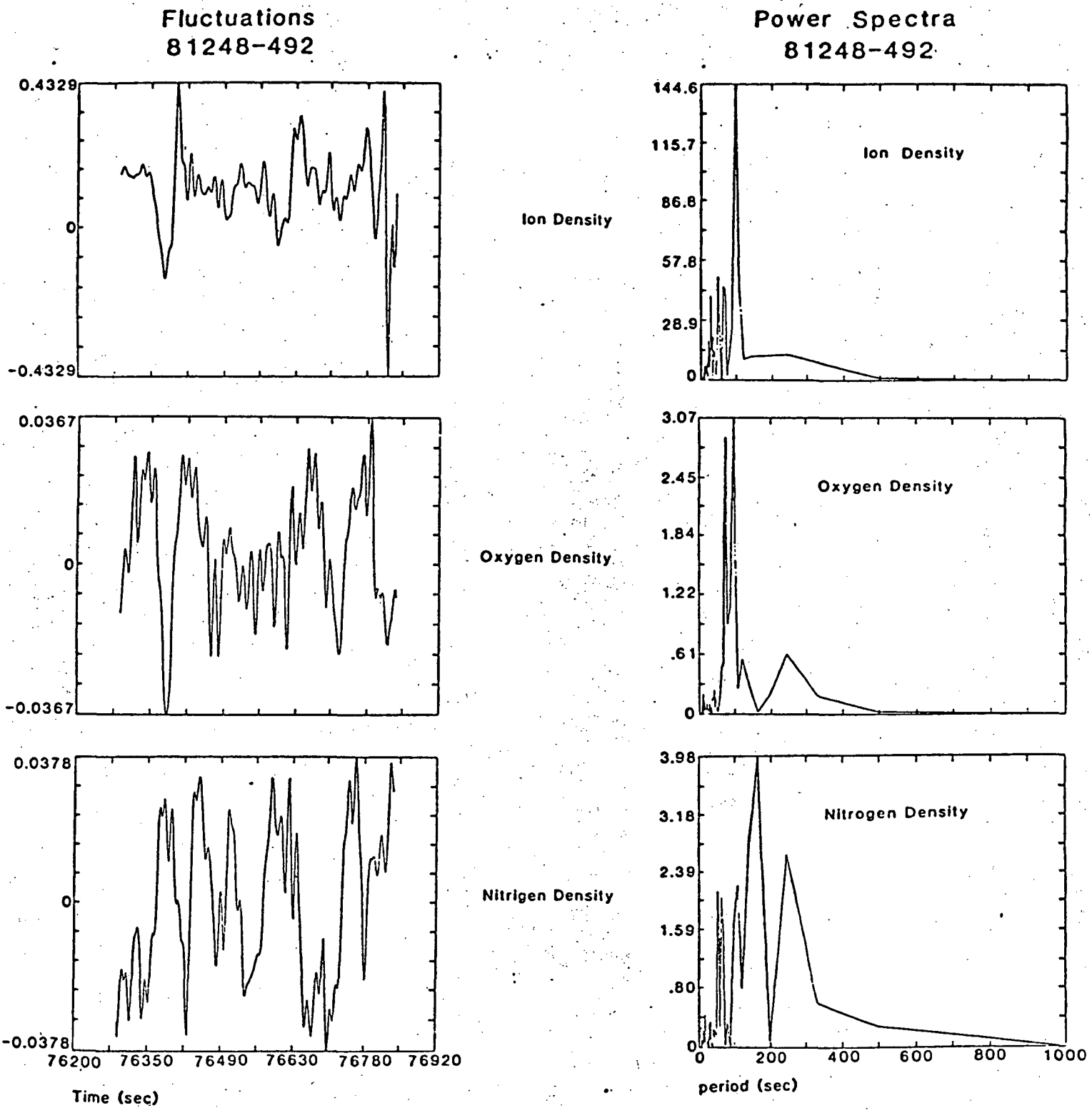

Fig. 6. Plots of fluctuations obtained by passing the logarithm of the ion, oxygen and nitrogen densities through a bandpass filter that passes structures with scale sizes from 90 to 1500 km. The plots are vs time in seconds UT. The data are for orbit 492 on day 81248.

Fig. 7. FFT spectra of the fluctuations in Figure 6 for day 81248. The spectra are plotted vs period in seconds.

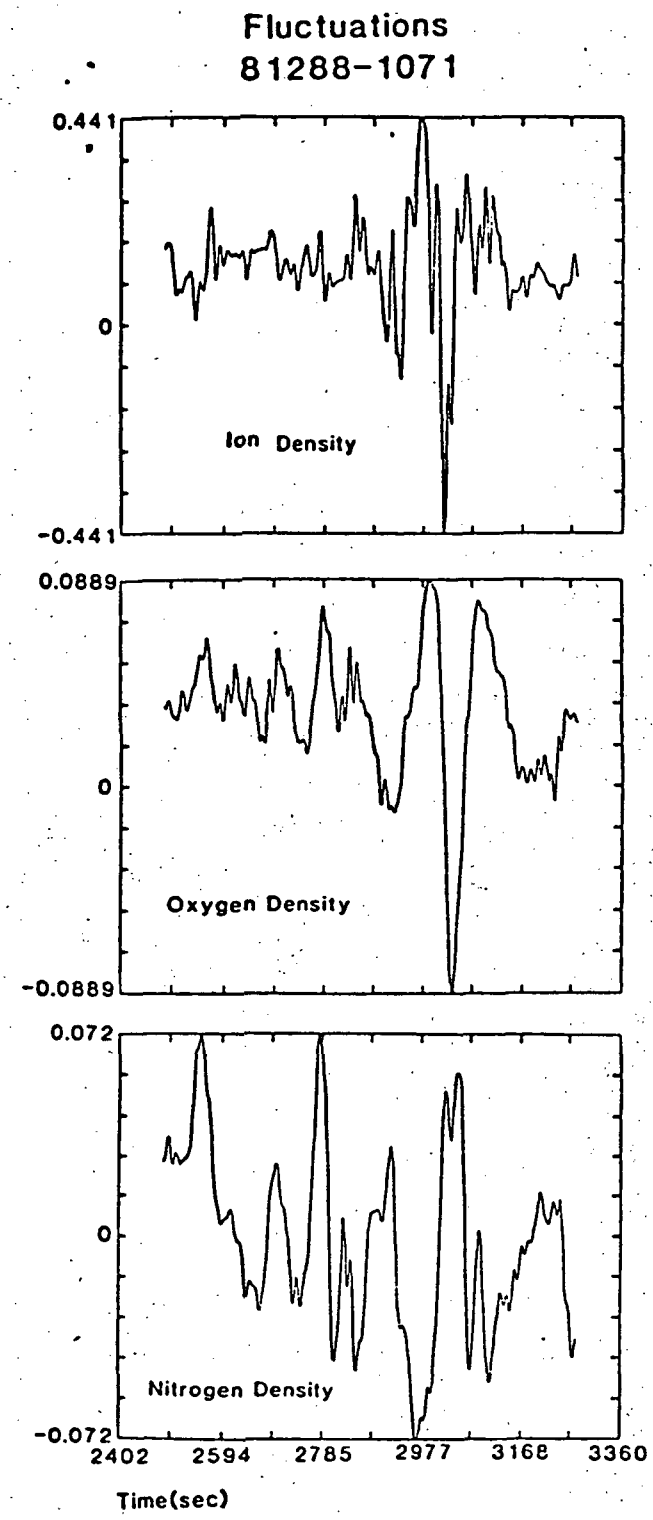

8. Same as Figure 6, but the data are for day 81288.

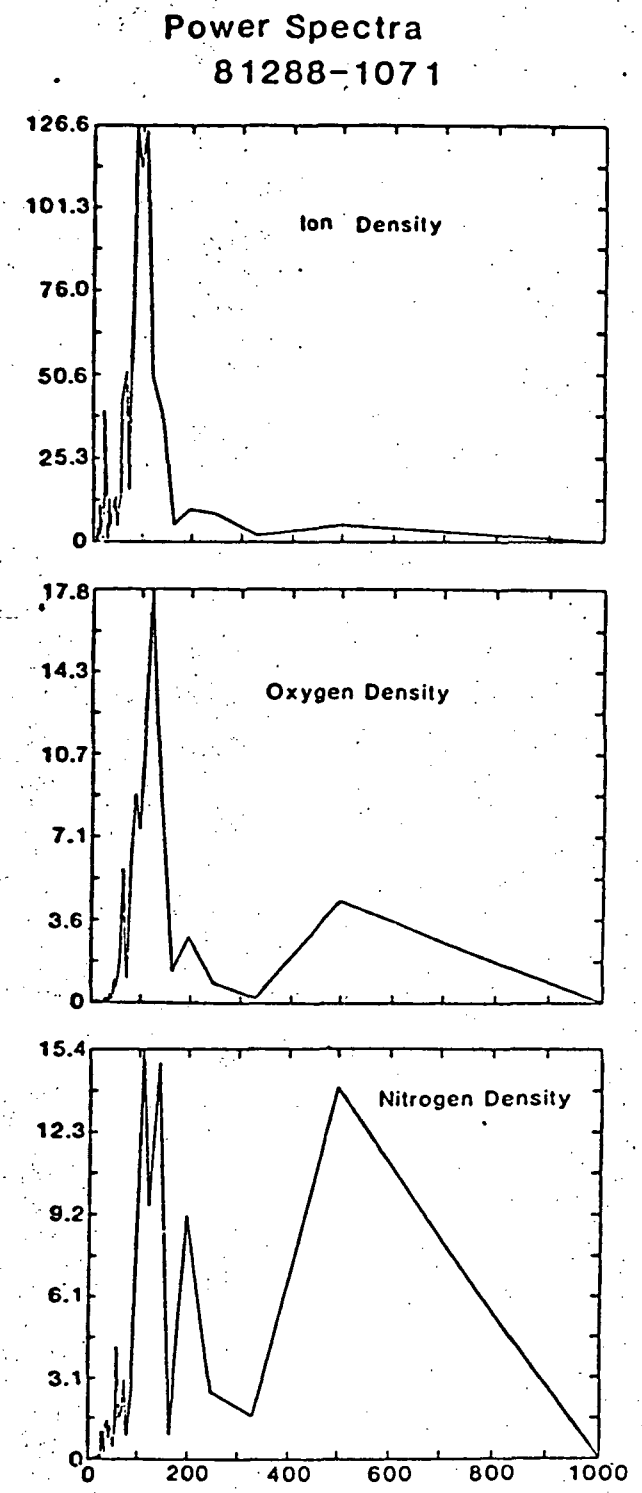

Fig. 9. Same as Figure 7, but for the data for day 81288.